Crustal Imbrication in an Alpine Intraplate Mountain Range: A Wide-Angle Cross-Section Across the Spanish-Portuguese Central System

I. DeFelipe[1,2] , P. Ayarza[2] , I. Palomeras[2] , M. Ruiz[1] , J. Andrés[3] , J. Alcalde[1] , D. Martínez Poyatos[4] , F. González Lodeiro[4], M. Yenes[2] , J. Elez[2] , I. Pérez-Cáceres[2] , M. Torne[1], and R. Carbonell[1]

[1]Geosciences Barcelona, GEO3BCN-CSIC, Barcelona, Spain, [2]Departamento de Geología, Universidad de Salamanca, Salamanca, Spain, [3]Institut Catogràfic i Geològic de Catalunya, Barcelona, Spain, [4]Department of Geodynamics, University of Granada, Granada, Spain

Abstract Intraplate ranges are topographic features that can occur far from plate boundaries, the expected position of orogens as described in the plate tectonics theory. To understand the lithospheric structure of intraplate ranges, we focused on the Spanish-Portuguese Central System (SPCS), the most outstanding topographic feature in the central Iberian Peninsula. The SPCS is an Alpine range that exhumes Precambrian-Paleozoic rocks and is located at >200 km from the northern border of the Iberian microplate. Here, we provide a P-wave velocity model based on wide-angle seismic reflection/refraction data of the central SPCS (Gredos sector). Our results show: (a) a layered lithosphere characterized by three major interfaces: Conrad, Mohorovicic, and Hales discontinuities, (b) an asymmetry of the crust-mantle boundary under the SPCS, (c) the extent of the Variscan batholith forming the main outcrops of Gredos, and (d) the thinning of the lower crust toward the south. This model suggests that the exhumation of the SPCS basement was driven by a south-vergent thick-skinned thrust system, developed in the southern part of the SPCS and that promoted crustal imbrication and a Mohorovicic discontinuity's offset under the SPCS. Thus, the deformation mechanisms of the crust seem to be controlled by the presence of the late- to post-Variscan granitoids that assimilated the Variscan mid-crustal detachment creating a new rheological boundary. This tectonic structure allowed the formation of Alpine crustal-scale thrust systems that eased coupled deformation of the upper and lower crust, leading to limited underthrusting of both crustal layers.

Plain Language Summary This study provides a lithospheric model of the Gredos sector of the Spanish-Portuguese Central System (SPCS), a mountain range located in the central Iberian Peninsula. Despite most of the Alpine deformation in the Iberian Peninsula was accommodated along the Iberian microplate borders (i.e., Pyrenees, Cantabrian Mountains, and Betics), shortening was also transferred toward the interior, forming the SPCS. This mountain building process brought igneous and metasedimentary rocks of the Precambrian-Paleozoic basement to the surface and contributed to the development of the Duero and Madrid Cenozoic basins, formed to the north and south of the SPCS. The SPCS exhibits a pop-up/pop-down structure with large-scale fault systems in its southern boundary, showing an asymmetric crustal structure with an offset of the crust-mantle discontinuity. The intrusion of granites during the Paleozoic had a large impact on the Alpine structure of the SPCS as they partially melted an older crust and erased previous discontinuities. Subsequently, the southern border of these granites represented weak zones that favored the nucleation of crustal-scale faults during the Alpine contraction. Ultimately, this process exhumed the SPCS over the Madrid Cenozoic basin.

1. Introduction

The structure of mountain belts reflects the mechanisms that accommodated the tectonic convergence in the lithosphere (Mouthereau et al., 2013). Orogenic belts are mostly located in the margins of continental plates (Dewey & Bird, 1970) and have been classically explained within the Wilson cycle (Wilson et al., 2019) by horizontal shortening, continental collision, and crustal thickening leading to basement exhumation. Despite the great advances in the knowledge of geodynamics processes achieved by the theory of plate tectonics, many features fall outside the Wilson cycle, such as deformation processes in intraplate regions (Heron et al., 2016). In fact, deformation

processes are not limited to the plate boundaries, and may extend to more than thousand kilometers away from the collision front (Ziegler et al., 1998) resulting in intraplate ranges. Contractional intraplate tectonic settings are the most diverse tectonic environments influenced by superimposed processes (e.g., Fernández-Lozano et al., 2011; Sokoutis & Willingshofer, 2011; Stephenson et al., 2009) and there is not a universally applicable model that explains the response of the intracontinental lithosphere to compression (Aitken et al., 2013). Therefore, the study of intraplate ranges is of key interest to unravel the lithospheric structure, and evolution of tectonic plates. Ultimately, understanding the mechanisms of intraplate deformation allows deeper knowledge of the conventional theory of plate tectonics and the origin of the current topography.

An outstanding geological setting to study intraplate deformation is the Spanish-Portuguese Central System (SPCS; Figure 1). The SPCS is a 700-km-long mountain range that represents the most prominent topographic feature of the central Iberian Peninsula and features altitudes locally higher than 2,500 m above sea level (a.s.l.). The SPCS has an E-W to NNE-SSW strike and is located at more than 200 km to the south of the Cantabrian Mountains, the Alpine mountain range formed by the northward subduction of the Iberian crust under the North Iberian margin (e.g., Gallastegui et al., 2016; Teixell et al., 2018). In addition, the Spanish part of the SPCS is bordered by foreland basins that feature a topographic difference between them of ∼400 m: (a) the Duero Cenozoic basin, to the north, is located on average at ∼800 m (a.s.l.), and (b) the Madrid Cenozoic basin, to the south, is located at ∼400 m (a.s.l.). The structure of the SPCS has attracted significant attention mainly due to its high topography in the interior of a tectonic plate. So far, research efforts have focused on finding models to explain the observed intraplate deformation (Cloetingh et al., 2002; De Vicente et al., 1996; de Vicente & Vegas, 2009; Vegas & Suriñach, 1987), the different tectonic and stratigraphic evolution of its foreland basins (de Vicente & Muñoz-Martín, 2013; Fernández-Lozano et al., 2011; Silva et al., 2017), its lithospheric structure (Andrés et al., 2019, 2020; Ayarza et al., 2021), and the tectonic origin of its topography (Casas-Sainz & de Vicente, 2009).

The lithospheric structure along the SPCS has been studied by natural and controlled source experiments since the 1980s. First, the SPCS was sampled by long-range controlled-source seismic experiments that provided rough estimations of the P-wave velocity distribution. These experiments also highlighted the heterogeneity of its lithosphere (Banda et al., 1981; Díaz et al., 1993), and revealed a moderate thickening of the crust under the SPCS (Suriñach & Vegas, 1988; Vegas et al., 1990; Vegas & Suriñach, 1987). Later, natural source experiments, potential field modeling (gravity and geoid; Gómez-Ortiz et al., 2005), and thermal analysis provided further constraints on the lithospheric architecture, revealing a thickening of the crust to 40 km and a Moho offset under the central SPCS (Andrés et al., 2019, 2020; Torne et al., 2015). However, controversy exists and two models are proposed to describe the crustal geometry of the SPCS and the contrasting topography between its two foreland basins. One model regards for lithospheric folding associated with an upper crust pop-up forming the main topographic relief in the Gredos sector of the SPCS (Cloetingh et al., 2002; de Vicente et al., 2018). This model implies a rheological stratification of the lithosphere with a weak and ductile lower crust underlain by a strong upper mantle (Fernández-Lozano et al., 2011; Muñoz-Martín et al., 2010). The second model proposed the formation of a crustal-scale south-vergent thrust system that exhumed the SPCS. This model implies the disruption of a pre-existing mid-crustal detachment and allows coupled deformation between the upper and lower crust (Andrés et al., 2019, 2020; Ayarza et al., 2021).

Notwithstanding the information provided by previous lithospheric studies, there are some questions that remain unsolved, such as: (a) the locus, geometry, and character of the lithospheric discontinuities, (b) their role in controlling the exhumation of the SPCS, and (c) the relationship between the Variscan granitoids and the style of mountain building and foreland basin formation. To shed light on the deep structure of the central part of the SPCS, a wide-angle (WA) seismic reflection/refraction experiment, CIMDEF (Central Iberian Massif Deformation), was acquired crossing the western part of the Duero Cenozoic basin, the Gredos sector of the SPCS, the western part of the Madrid Cenozoic basin and the northernmost part of the Toledo Mountains (Figures 1 and 2). The data acquired have allowed us to construct a P-wave velocity (Vp)-depth model and to define the major crustal and lithospheric mantle discontinuities. Complementary to the lithospheric Vp model, this dense seismic network recorded a wealth of natural and anthropogenic seismic noise sources, highlighting its utility beyond modeling the subsurface structure (Díaz et al., 2022).

The Vp distribution and the locus of the lithospheric discontinuities are assets to resolve the crustal deformation mechanisms active during the Alpine contraction and have allowed us to evaluate the role of the crustal-scale
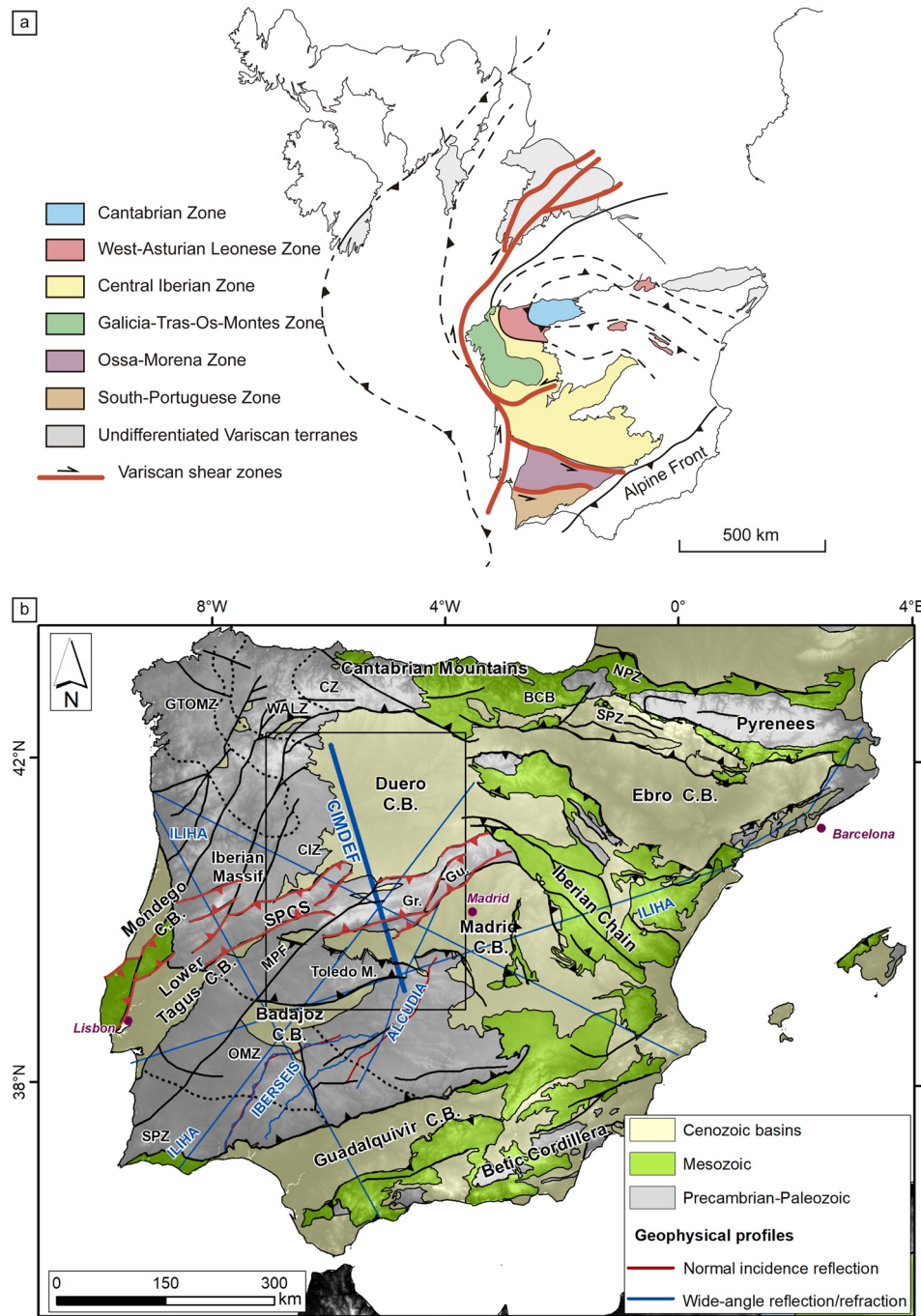
Figure 1. (a) position of the Iberian Peninsula and the zonation of the Iberian Massif for the end of the Variscan orogeny (after Martínez Catalán et al., 2002; 2007); (b) Simplified geological map of the Iberian Peninsula with the main deep seismic sounding profiles acquired along the Iberian Massif. The black square shows the location of the geological map of Figure 2. The Spanish-Portuguese Central System (SPCS) is indicated by red lines, with the location of the Gredos and Guadarrama sectors (Gr. and Gu., respectively). Dotted black lines represents the zones of the Iberian Massif (CIZ, Central Iberian zone; CZ, Cantabrian zone; GTOMZ, Galicia-Trás-os-Montes zone; OMZ, Ossa-Morena zone; SPZ, South Portuguese zone; WALZ, West Asturian-Leonese zone). BCB, Basque-Cantabrian Basin; MPF, Messejana-Plasencia fault; NPZ, North Pyrenean Zone; SPZ, South Pyrenean Zone; Toledo M., Toledo Mountains. Cenozoic basins are simplified as C.B. The topography is from CIAT-CSI SRTM (Jarvis et al., 2008). Geological map simplified from Rodríguez Fernández et al. (2015) and the Alpine tectonic framework from de Vicente et al. (2018, 2021).

Alpine faults in the exhumation of this intraplate mountain range. Moreover, our Vp model complements previous lithospheric models based on global-phase seismic interferometry and ambient seismic noise (Andrés et al., 2019, 2020), helping to resolve the crust and upper mantle geometry of Gredos.

2. Setting

2.1. Geology of the Study Area

The SPCS is an Alpine mountain range that crosses the Iberian Massif, the westernmost outcrop of the Variscan orogen in Europe (e.g., Díaz Alvarado et al., 2013; Martínez Catalán et al., 2014). The Iberian Massif is classically divided in six zones (Pérez-Estaún and Bea, 2004; Simancas, 2019) that from north to south are: Cantabrian, West Asturian-Leonese, Galicia-Trás-os-Montes, Central Iberian, Ossa-Morena, and South Portuguese zones (Figure 1a). Regarding their paleogeographic affinity, the Cantabrian, West Asturian-Leonese, and Central Iberian zones represent the Paleozoic margin of Gondwana (Martínez Catalán et al., 1997; Pérez-Estaún et al., 1988) whereas the Galicia-Trás-os-Montes zone is completely allochthonous over the Central Iberian zone (CIZ; Arenas et al., 2014; Martínez Catalán et al., 1997). In the SW of the Iberian Peninsula, the Ossa-Morena zone is interpreted as a continental piece that rifted from Gondwana in the Early Paleozoic (Matte, 1991), and the South Portuguese zone is usually correlated with the Rheno-Hercynian zone of Central Europe (Franke & Dulce, 2017; Pérez-Cáceres et al., 2017). The study area and where the SPCS is located corresponds to the CIZ.

The CIZ is formed by the Neoproterozoic-Lower Cambrian Schist-Graywacke complex, a thick succession of shale and graywacke with intercalations of other sedimentary and volcaniclastic rocks (Rodríguez Alonso et al., 2004; Talavera et al., 2015), lower-middle Cambrian sedimentary rocks, and Lower Ordovician quartzite that unconformably overlie the previous successions (Talavera et al., 2012). Toward the northern and easternmost parts of the CIZ, subvolcanic and volcano-sedimentary rocks are partly intercalated with the Early Ordovician sediments (García-Arias et al., 2018; Montero et al., 2009). Ordovician to Silurian slates and quartzite conformably overlie the previous successions (Diez-Montes et al., 2010) and the Devonian and Carboniferous sedimentary sequences crop out scarcely (Gutiérrez-Marco et al., 2019). All of these sequences are intruded by huge volumes of late Carboniferous-early Permian granitoids, which allowed for a magmatic classification from north to south into: Zone I, with negligible volume of granitoids; Zone II, with a vast volume of granitoids; and Zone III, where granitoids are less abundant (Simancas et al., 2013; Figure 2). The granitoids in the Spanish part of the SPCS correspond to the Ávila or Central System batholith, one of the largest batholiths in the European Variscan orogen (e.g., Villaseca et al., 2012). It is composed mainly by monzogranite, granodiorite and leucogranite whose crystallization ages have been estimated between 330 and 289 Ma (Bea et al., 2003; Díaz-Alvarado et al., 2012; Martínez Catalán et al., 2014; Orejana et al., 2012). These granitoids were preceded by volumetrically insignificant mafic-ultramafic calc-alkaline rocks and postdated by lamprophyre dykes (Bea, 1985; Bea et al., 1999; Orejana et al., 2008). In addition, anatectic complexes (or thermal domes) formed mainly by gneiss, migmatite, granitoid and minor ultramafic, mafic and intermediate rocks, crop out in the central part of Gredos (e.g., Peña Negra anatectic complex), and in the Toledo Mountains (Bea et al., 2006; Bea & Pereira, 1990; Castiñeiras et al., 2008; Hernández Enrile, 1991; Pereira Gómez & Rodríguez Alonso, 2000).

The Permian-Mesozoic cover of the basement in the Spanish sector of the SPCS crops out very locally. The SPCS separates two Cenozoic basins, the Duero (to the north) and Madrid (to the south) basins (Figures 1b and 2), filled by conglomerate, sandstone, limestone, and gypsum (De Vicente et al., 2011). These basins feature up to 3 km of sediments in the Duero Cenozoic basin (Gómez-Ortiz et al., 2005), and up to 3.8 km in the Madrid Cenozoic basin, close to the SPCS (de Vicente & Muñoz-Martín, 2013). In addition, smaller Cenozoic subbasins are distributed across the SPCS (Cunha, de Vicente, et al., 2019), classified as thrust basins related to low-angle thrusts, or as transtensional basins related to the high-angle left-lateral Messejana-Plasencia fault (De Vicente et al., 2011).

2.2. Geodynamic Evolution

The Precambrian rocks of the Iberian Massif were variably imprinted by the Cadomian orogeny (late Neoproterozoic) (Álvaro & Lorenzo, 2021) that took place along the northern margin of Gondwana (Cambeses et al., 2016).
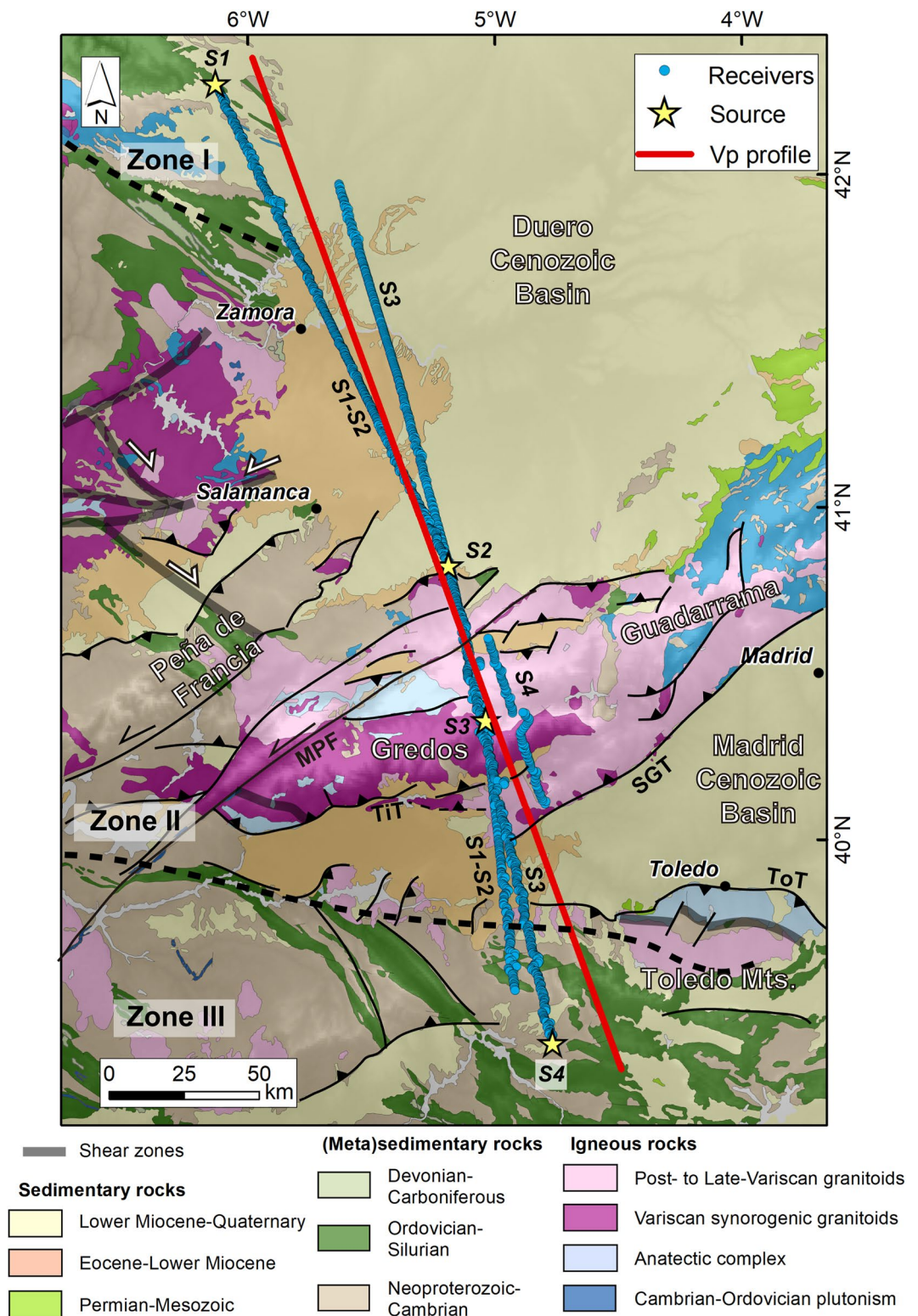
Figure 2. Detailed geological map of the study area (black rectangle in Figure 1) including the location of the shots (S1–S4), receivers (blue circles), and the projected profile (red line). The S1–S4 labels along with the receivers' positions indicate the acquisition geometry for each shot. Dashed black lines separate zones I, II, and III according to the presence of granitoids (Simancas et al., 2013). MPF, Messejana-Plasencia fault; SGT, South Gredos thrust; TiT, Tiétar thrust; ToT, Toledo thrust. The topography is from CIAT-CSI SRTM (Jarvis et al., 2008) and the geological map from Rodríguez Fernández et al. (2015).

The related subduction resulted in arc-related magmatism (mainly in the Ossa-Morena zone; Bandrés et al., 2004) and thick flysch volcano-sedimentary sequences (e.g., the Schist-Graywacke complex in the CIZ; Rodríguez Alonso et al., 2004) deformed by gentle folds (Talavera et al., 2015). Since the middle-late Cambrian, rifting related to the opening of the Rheic Ocean resulted in passive margin sedimentation in the northern margin of Gondwana from the Early Ordovician to the Middle Devonian (Gutiérrez-Marco et al., 2019). The closure of the Rheic Ocean during the Devonian and the collision of the passive margin of Gondwana with Laurussia, forming the Pangea supercontinent, culminated in the Variscan orogen (Kroner et al., 2016; Matte, 2001; Nance et al., 2012). The Variscan orogeny produced crustal thickening in the internal zones of the Iberian Massif during the early Carboniferous, followed by thermal weakening and gravitational collapse in the middle Carboniferous, exhuming the Variscan orogenic roots (Rubio Pascual et al., 2016).

In the central and northern parts of the Iberian Massif, the Variscan deformation yielded three generations of contractional (C1, C2, and C3) and two extensional (E1 and E2) structures (Martínez Catalán et al., 2014). The stages C1, C2, and E1 partly overlap, with the age of each deformation phase being progressively younger from the CIZ toward the Cantabrian zone (e.g., Dallmeyer et al., 1997; Dias da Silva et al., 2021). C1 (dated in the CIZ between 360 and 350 Ma; Azor et al., 2019; Martínez Catalán et al., 2014) is characterized by a heterogenous deformation with recumbent and upright folds (e.g., Diez Balda et al., 1990) and is the response of the arrival of the Variscan tectonic front to the autochthonous terrains (Dias da Silva et al., 2021). The second contractional event (C2, dated in the CIZ in 345–330 Ma; Azor et al., 2019; Martínez Catalán et al., 2014) resulted from thrusting the allochthonous piles of the Galicia-Trás-Os-Montes zone toward the SE (present-day coordinates). The crustal thickening created during C1 and C2 triggered synorogenic extensional collapse during the first extensional episode (E1, dated in the CIZ in 330–315 Ma; Alcock et al., 2015; Azor et al., 2019; Martínez Catalán et al., 2014) and gneiss and migmatite-cored domes formed bounded by low-angle extensional detachments and shear zones. The third contractional Variscan stage (C3) produced vertical or steeply inclined folds with some of the largest folds nucleated on E1 domes (315–300 Ma; Azor et al., 2019; Martínez Catalán et al., 2014). A second extensional Variscan stage (E2, extended to 300 Ma; Azor et al., 2019; Martínez Catalán et al., 2014), partly coeval with C3 toward the northern part of the CIZ, produced extensional detachments, exposed high-grade metamorphic rocks and formed new domes. During the extensional stages the Peña Negra anatectic complex (peak age of migmatization of 335–305 Ma; Díaz Alvarado et al., 2013; Montero et al., 2004); and shear zones west and southwest of the city of Salamanca developed (Diez Balda et al., 1995; Díez Fernandez & Pereira, 2017; Escuder Viruete et al., 1994, 2000; González-Clavijo & Díez Montes, 2008; Gutiérrez-Alonso et al., 2015). The last compressional Variscan stage, C3, has been assigned to oroclinal bending (Martínez Catalán, 2011, 2012; Weil et al., 2019). Most of the Variscan magmatism of the Central System batholith is contemporary with C3 and E2 phases (Bea et al., 2003; Díaz Alvarado et al., 2013; Orejana et al., 2012; Zeck et al., 2007).

The onset of the break-up of Pangea occurred during the Permian-Triassic rifting stage with a generalized subsidence and basin formation (López-Gómez et al., 2019). After that and until the mid-Cretaceous, the Iberian Peninsula acted as a passive margin during the spreading of the North Atlantic Ocean. A widespread Early Jurassic magmatic event was related to the onset of the Central Atlantic Ocean (e.g., Vegas, 2000; Wilson, 1997). One of the expressions of this magmatic event in the Iberian Massif is the 530 km long Messejana-Plasencia dolerite dyke, dated to 203 ± 2 Ma (Dunn et al., 1998), that crosses Gredos (Figures 1 and 2). This Mesozoic rifting event determined the Iberian microplate boundaries and generated thick sedimentary basins specially in the north and east of the Iberian Peninsula (e.g., Alonso et al., 1993; Cadenas & Fernández-Viejo, 2017; DeFelipe et al., 2017; Martín-Chivelet et al., 2019; Quijada et al., 2014).

From the Late Cretaceous to the present, the relative movements between the African, Iberian, and European plates in the context of the Alpine contraction, gave rise to the current mountain ranges in the Iberian Peninsula (e.g., Macchiavelli et al., 2017; Rosenbaum et al., 2002). Accordingly, the SPCS was exhumed since the middle Eocene (De Bruijne & Andriessen, 2002; de Vicente et al., 2018) resulting in the current intraplate mountain range configuration. The SPCS represents a large thick-skinned basement pop-up with NE-SW and E-W oriented thrusts (de Vicente et al., 2018), separated by tectonic depressions or pop-downs (de Vicente et al., 2007). During the Cenozoic intraplate deformation, the crustal-scale, left-lateral strike-slip Messejana-Plasencia fault nucleated the homonymous dyke (de Vicente et al., 2018, 2021; Villamor, 2002), with tectonic activity until the Holocene and a

Table 1
Data Acquisition Instrumentation and Parameters for Each of the Shots

Description	Source S1	Source S2	Source S3	Source S4
Acquisition date	June 2019	June 2019	June 2017	May 2012
Recording instruments	750 UNITE-RAU 1-C; 250 UNITE-RAU 3-C	750 UNITE-RAU 1-C; 250 UNITE-RAU 3-C	580 Reftek 125a TEXANS	110 Reftek 125a TEXANS
Sensor frequency	4.5 Hz 1C and 10 Hz 3C	4.5 Hz 1C and 10 Hz 3C	4.5 Hz 1C	4.5 Hz 1C
Offset range	0–333 km	−181 to 156 km	−191 to 91 km	−136 to −80 km
Receiver spacing	400 m	400 m	400 m	400 m
Charge size	1,000 kg	1,000 kg	1,000 kg	1,000 kg
Source configuration	One borehole 60 m depth	One borehole 60 m depth	One borehole 60 m depth	One borehole 60 m depth

horizontal displacement of ∼ 1-5 km (Villamor et al., 1996, 2012; Villamor, 2002). In addition, intramontane Cenozoic sedimentary basins formed as pull-apart basins related to E-W and NE-SW thrusts (de Vicente et al., 2021).

The exhumation of the SPCS is accompanied by the evolution of the fluvial network in the surrounding basins with a transition from endorheic to exorheic conditions (e.g., Cunha, Martins, et al., 2019; Rodríguez-Rodríguez et al., 2020). During the later exorheic evolution, the Duero and Madrid Cenozoic foreland basins experienced different fluvial incision rates which maximum values have been estimated in 220 m/2.23 ka and 165 m/1.99 ka (average downcutting rates of *ca.* 99 and 83 mm/ka) in the Madrid and Duero Cenozoic basins, respectively (Silva et al., 2017).

3. Data and Methods

3.1. Data Acquisition

The Vp model presented here is based on WA seismic reflection/refraction data of four shot records acquired in different time slots (Table 1 and Figure 2). As part of the CIMDEF project, in 2017, we recorded shot S3 along an NNW-SSE transect. Logistical issues forced the interruption of the acquisition and two originally planned shots were not detonated. In this phase, 580 TEXANS from the IRIS PASCAL pool were deployed. In 2019, and also within the CIMDEF initiative, we recorded shots S1 and S2 along a largely overlapping NNW-SSE transect. An additional source point was planned in the southern end, but it could not be acquired due to permission issues. In this second phase, we deployed 750 one-component UNITE RAU instruments from CGG and 250 GEO3BCN-CSIC three-component UNITE RAU. To complete the data set, we were also able to use a shot record (S4) acquired in 2012 as part of the ALCUDIA-WA experiment (Ehsan et al., 2015). This shot was registered by a reduced number of stations along an N-S transect across the SPCS. The specific acquisition parameters are detailed in Table 1.

3.2. Data Processing

The processing applied to the shot records was designed to emphasize the arrivals and attenuate the environmental noise. Amplitude corrections were applied to recover the spherical divergence loss of energy and the amplitude variations caused by offset. The recorded traces were later normalized by the root mean squared (rms) of the background noise, picked at the last 1-s long window of the record. The signal shows a fairly white spectrum in the 3–55 Hz frequency band. The highest energy contributions come from the most prominent phases (Pg, PmP, and Pn) all within the 5–35 Hz frequency band. Due to the acquisition logistics of this experiment, receivers and sources are not strictly aligned and to obtain a Vp model, they have been projected along a single line that crosses the SPCS (Figure 2). Offsets have been kept constant for the projection.
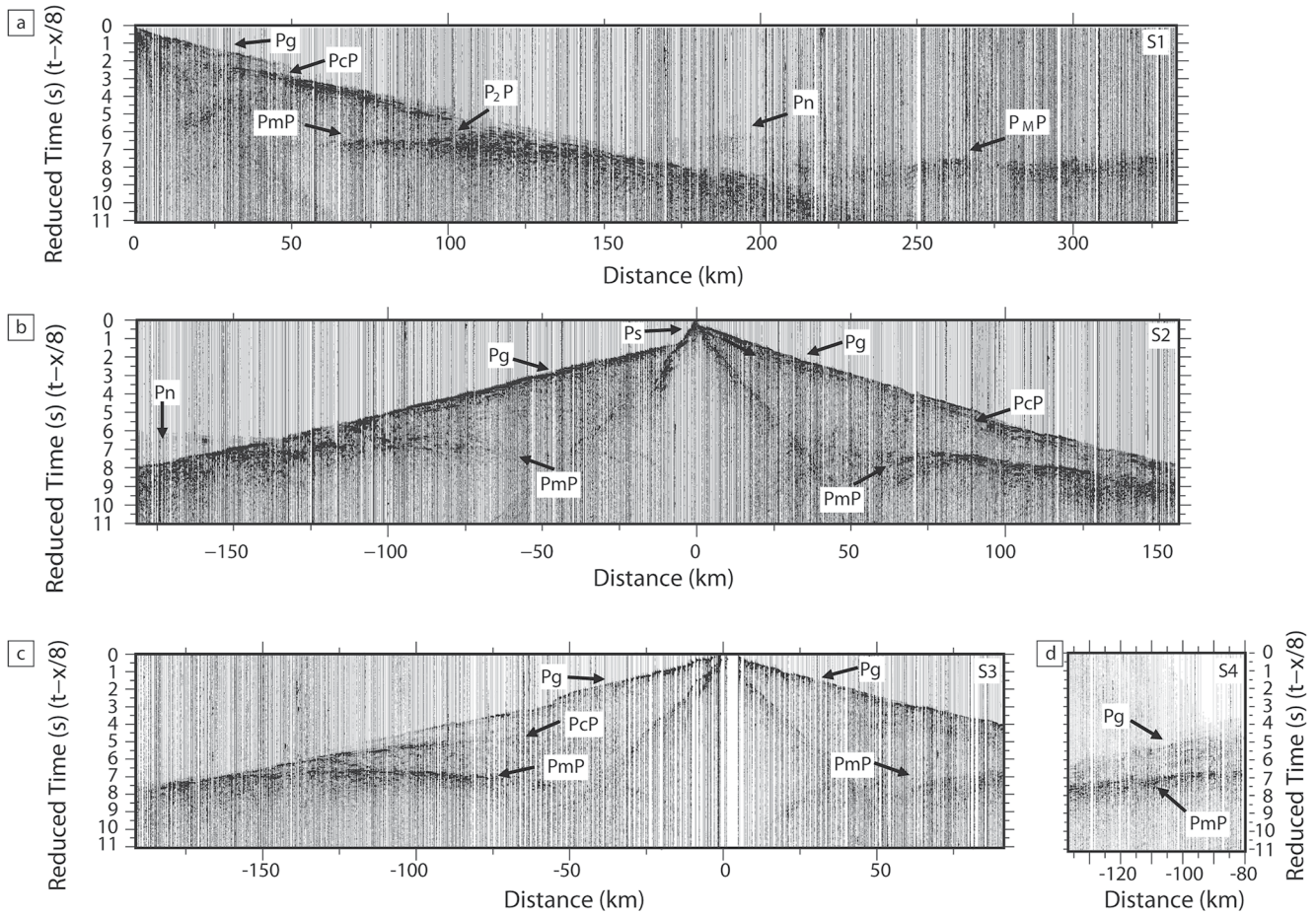
Figure 3. Vertical component shot records displayed at reduced time (reduction velocity of 8 km/s). The data have been band-pass filtered at 2–25 Hz. The arrivals are labeled as: Ps (direct arrival sampling the sedimentary basin), Pg (seismic phase sampling the basement), PcP (reflection at the top of the lower crust), P_2P (a reflection within the lower crust), PmP (Moho discontinuity reflection), Pn (upper mantle head wave), and P_MP (upper mantle internal reflection).

3.3. Phase Identification and Data Description

The high spatial density that characterizes this data set allows us to identify clear phases to base our model: Ps (direct arrival in sediments), Pg (direct arrival in the basement), PcP (reflection at the top of the lower crust), P_2P (reflection within the lower crust), PmP (Moho reflection), Pn (head wave within the upper mantle), and a very prominent P_MP (upper mantle reflection). Figure 3 shows a plot of the vertical component of the shot records at a reduced time using a velocity of 8 km/s *versus* offset (distance from source to receiver). Negative offsets correspond to receivers located to the north of the shot location (left side of the figures), whereas positive offsets correspond to arrivals located to the south (right side of the figures) of the source location.

Shot gathers show a clear P-wave arrival for the upper and lower crust, the Moho discontinuity, and the upper mantle (Figure 3). The direct arrivals (Pg) and the reflected P-wave arrivals at the Moho (PmP) are the most outstanding events and are identified in all the shot gathers. In S1 (Figure 3a), the Pg phase can be followed up to an offset of 60 km, featuring lower amplitude beyond this distance. Below the Pg phase, the PcP reflection is identified at offsets between 25 and 100 km. Below the PcP, a burst of energy (labeled as P_2P) is identified at offsets from 90 to 120 km. The P_2P phase reflects the existence of a structure in the lower crust under the Duero Cenozoic basin. Immediately after P_2P, the PmP phase, the Moho reflection, consists of a laterally coherent energy band with a >0.5 s twtt (two-way travel time) coda, visible from offsets of 70–130 km. The Pn phase, refracted with the critical angle in the upper mantle, appears as a relatively weak but identifiable first arrival at offsets of between 150 and 230 km, and at 6 s twtt in the reduced time shot gather. The last phase identified is the

P_MP, a high amplitude laterally coherent reflection in the upper mantle with a >1 s twtt coda, visible at distances beyond an offset of 200 km and at approximately 7 s twtt.

In S2 (Figure 3b), a marked Ps phase (direct wave in the sediments of the Duero Cenozoic basin) is identified at negative offsets and for a few tens of kilometers. The Pg phase appears as a well-defined laterally continuous first arrival. It can be followed to an offset of −130 km to the north of the shot point and 100 km to the south. After the Pg phase, the reflection in the top of the lower crust, the PcP phase, has been only identified at positive offsets (>100 km). The PmP phase can be followed from offsets of −130 km to −75 km at 6.5 s twtt in the reduced time shot gather, and at offsets from 50 km to the end of the shot record. At positive offsets, the PmP phase shows a complex hyperbolic geometry, featuring a superposition of at least two branches, and appearing at later times than the equivalent phase to the north. Furthermore, this phase does not become asymptotic with the first arrivals (Pg) at large offsets in the southern part, as it happens to the north. The striking asymmetry of the PmP at both sides of the source indicates a marked change in the deep crustal structure to the north and south of S2. Finally, the Pn phase is identified as the first arrival from an offset of approximately −140 km and at 6.7 s twtt.

In S3 (Figure 3c), the Pg phase is rather continuous at positive and negative offsets, but at an offset of −60 km and at 3 s twtt, a delay in the first arrival is identified. This corresponds to the boundary between the basement and the Duero Cenozoic basin (Figure 2). Below the Pg phase, the reflection in the top of the lower crust, PcP, is identified to the north of the shot point as a ∼0.1 s twtt coda event at offsets between −70 and −130 km. This phase cannot be traced at positive offsets probably due to limited sampling (<100 km offset). The subsequent arrival corresponds to the PmP phase, a relatively sharp (0.3 s twtt coda) event identified between offsets of −70 and −160 km and at 7 s twtt. In contrast, the PmP phase at positive offsets (south) is relatively diffuse. There, it has an almost 2 s twtt coda and can be traced from an offset of 50 km and at 7.5 s twtt to the end of the section.

S4 (Figure 3d) is a short offset shot gather recorded along a 55 km long profile across the SPCS. This shot provided relatively limited information, with the Pg phase and a high amplitude and marked PmP phase. At the recorded offset range, PmP dips to the north and has a ∼1.5 s twtt coda. Note that at similar offsets, PmP appears as a nearly horizontal phase in shot gathers S1 and in the northern part of S3, further supporting (as in S2) a Moho and/or crustal asymmetry.

3.4. Interpretation Procedure

To construct a two-dimensional Vp model, first arrivals were picked and travel times were modeled using a ray tracing-based utility (Zelt & Smith, 1992). The travel time picks were selected for each phase at the onset of high amplitude events. Due to the complexity of the data, the model was obtained by forward modeling, using a trial and error approach for each shot and then combined into a single model that accounts for all arrivals. This interpretation procedure performs iterative ray tracing travel-time calculations with a parameterization based on velocity and boundary nodes to reckon the Vp model. A layer striping strategy was followed by using the Ps and Pg arrivals to constrain the velocity of the upper crust. The lower crust phase was then included, followed by the Moho and the subcrustal discontinuity.

The initial model was defined by the topography along the transect, the projection of the shot records along the line maintaining the offset, and four layers: sedimentary basin, upper crust, lower crust, and upper mantle. The initial model included information coming from previous studies along the study area (Andrés et al., 2019, 2020; Ayarza et al., 2010). Subsequently, velocity and boundary nodes were adjusted until a reasonable fit with the observed travel time was reached (±0.25 s), tracing refracted, reflected, and head waves rays for all the layers. The resulting Vp model is plotted after smoothing and shows the superposition of iso-velocity contours drawn every 0.2 km/s (Figure 4).

4. Results: Vp Model

4.1. Vp Model Description

The Vp model presented in this work can be laterally divided into three parts considering the different geological domains in the study area (Figure 4).
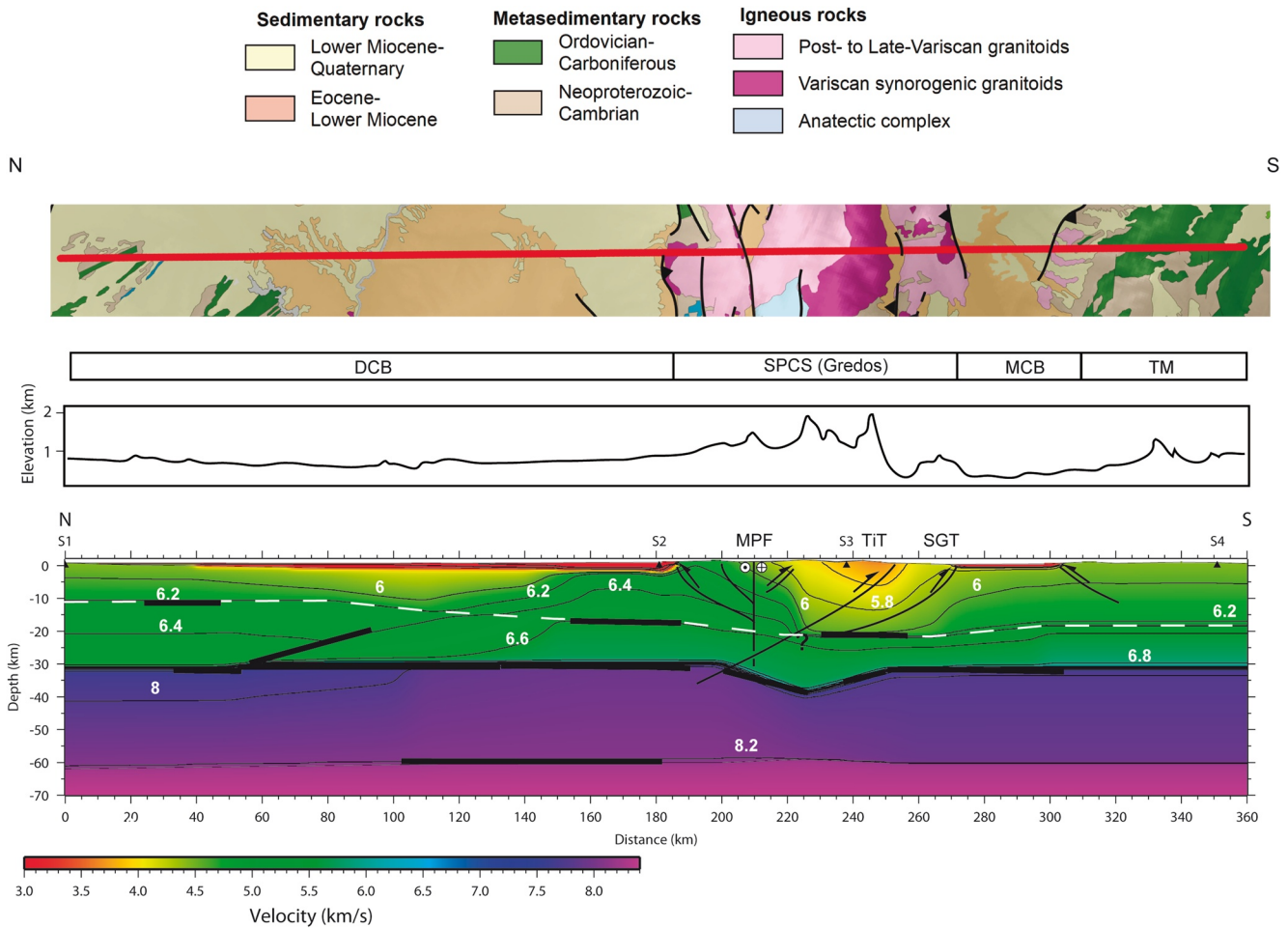
Figure 4. Vp model of the study transect with iso-velocity lines (km/s). Bold lines show the interface segments constrained by the data and the broken white line the modeled position of the Conrad discontinuity. The topography along the profile and the geology of the area are also represented. DCB, Duero Cenozoic basin; MCB, Madrid Cenozoic basin; MPF, Messejana-Plasencia fault; SGT, South Gredos thrust; SPCS, Spanish-Portuguese Central System; TiT, Tiétar thrust; TM, Toledo Mountains. S1 to S4 are the sources.

The northern part covers the first 180 km approximately, the Duero Cenozoic basin. Its Cenozoic sediments are modeled with a vertical velocity gradient from 3 to 4.2 km/s, with a maximum thickness of 3 km in the southern border. The velocity in the upper crust varies laterally ranging from 5.7 to 6.2 km/s in the top to 6.2 to 6.5 km/s in the base. The top of the lower crust deepens toward the south, from 10.5 to 17 km. The lower crust features velocity gradients of 6.3–6.6 km/s in the top to 6.5–6.7 km/s in the base. Despite the low velocity for the lower crust modeled in the northernmost part of the profile, the Vp jump and the reflection identified in S1 (Figure 3a) eased the identification of the Conrad discontinuity (Finlayson et al., 1984; Wever, 1989). The base of the crust is horizontal at 30–31 km depth and implies a Vp increase to 7.9–8.0 km/s. A lithospheric mantle discontinuity sampled by the P_MP phase is modeled as a boundary at 59–60 km depth under the Duero Cenozoic basin, featuring a velocity contrast from 8.2 to 8.3 km/s.

The central part of the profile comprises the interval from 180 to 270 km, that is, the SPCS area. There, the upper crust is characterized by significant lateral Vp variations ranging from 5.5 to 6.1 km/s in the top, and from 6 to 6.6 km/s in the base. The lateral variation in the Vp reveals, between offsets of 110–225 km, a dome-shaped geometry characterized by undulated iso-velocity contours, with a steep inclination in the southern edge and a gentle inclination to the north. The lower crust is characterized by a velocity of 6.6 km/s in the top and 6.7 km/s in the base. The top of the lower crust dips toward the south from a depth of 17 to 21.5 km. The crust-mantle boundary reaches 39 km depth under the Gredos sector (225 km along the profile). This increase in the crustal thickness is achieved by a ramp located between 200 and 225 km.

The southern part of the profile goes beyond 270 km and covers the Madrid Cenozoic basin and the Toledo Mountains. Despite possible uncertainties in this area (see Section 4.2), the modeled thickness of the Madrid Cenozoic basin is less than 1 km and the velocities grade from 4 to 4.3 km/s. The upper crust shows a constant increase of velocities with depth, from 5.8 to 6.2 km/s. The velocities of the lower crust grade from 6.5 to 6.8 km/s. The thickness of the lower crust decreases to 13 km and the Moho discontinuity lies at ~31–32 km depth.

The model described above shows that along the profile, the Vp distribution features significant lateral changes. The main outcropping rocks in this part of the SPCS are granitoids, a lithology with Vp values that range between 5.6 and 6.6 km/s (e.g., Birch, 1960). These velocities are consistent with those of Carboniferous granitoids studied along the IBERSEIS profile (see location in Figure 1b). There, high velocities are registered in the cores of the batholiths (fresh rock), and low velocities in the aureoles, as well as in altered or fractured zones within the granites (Flecha et al., 2006). Therefore, the dome-shaped iso-velocity contours may be somehow related to the complex late-Variscan igneous intrusions cropping out in the SPCS. The prolongation at depth of this dome-shaped morphology also reveals high Vp in the lower crust. These high velocities are consistent with the presence of granulite and other high-grade metamorphic rocks, and/or mafic rocks (e.g., Brown et al., 2003; Chroston & Evans, 1983; Manghnani et al., 1974), which are also mapped in the Central System batholith (Bea et al., 1999). In fact, restite, a residual source material common in granite (Chappell et al., 1987), is present in the SPCS (Castiñeiras et al., 2008). It forms after granite melt extraction or segregation during the Variscan anatexis (e.g., Pereira González & Rodríguez Alonso, 2000; Villaseca et al., 1999) and accumulates in the lower crust. The existence of mafic rocks in the Messejana-Plasencia dyke also brings the question of its implication in the Vp structure of the crust. Unfortunately, the resolution and characteristics of the method used here are not geared to identify a vertical change in the Vp caused by the dyke, whose width ranges from 5 to 200 m (Cebriá et al., 2003). Additionally, the phase labeled as P_2P in S1 (Figure 3a) may indicate a north-dipping structure in the lower crust. This interface may correspond to a change in the physical properties of that part of the lower crust of an unknown origin.

Along the study profile and toward the southern half of the Gredos sector, a remarkable decrease of the Vp is modeled. This Vp reduction may reflect a change in the composition of the basement linked to the lithological variability of the igneous rocks described for the Central System batholith (Bea et al., 1999, 2003). Toward the Toledo Mountains, the Vp increases progressively with depth and no major lateral variations are modeled, although this part of the model is the least constrained. The Vp model also reveals that the lower crust is thinner toward the south, ranging from approximately 20-km thick at the northern end of the profile to 13-km thick at the southern end.

The prominent P_MP phase reveals the existence of a conspicuous upper mantle discontinuity, probably a few kilometers thick. This arrival has been identified previously in other areas of the Iberian Massif (Ayarza et al., 2010; Díaz et al., 1993; Palomeras et al., 2009; Palomeras, Ayarza, et al., 2021) and has been explained as the reflection of a layered or gradient transition zone consistent with the spinel-lherzolite to garnet-lherzolite transition (Ayarza et al., 2010; Palomeras, Ayarza, et al., 2021), attributed to the Hales discontinuity. To our knowledge, the continuity, reflectivity, and length of this phase are unprecedented, not only in the Iberian Massif but probably at a worldwide scale.

4.2. Model Uncertainties and Resolution

The Vp model (Figure 4) reproduces the travel-time branches identified in all shot records (Figure 5). However, the observed misfits are expected since there are several factors that contribute to the mismatch between the modeled and observed travel times. The projection onto a straight line of a complex acquisition pattern (Figure 2) and the rough topography along the study transect (variations of up to ~1,600 m) produce small misfits. Note that along the ALCUDIA-WA profile (see location in Figure 1), altitude variations of only 150 m have yielded travel-time errors of <0.05 s, assuming a Vp of 3 km/s (Ehsan et al., 2015). Additionally, small-scale features like near-surface structures, irregularities of the batholith boundaries, and local existence of metasedimentary rocks may be below the resolution of the method and introduce local variations in the velocity field. Another consideration is that the SPCS strike changes from an E-W to a NE-SW orientation along the modeled transect, south of S3, possibly inducing misfits at depth. In summary, the geologically complex 3D structure of the SPCS and its crustal heterogeneity contribute to the uncertainties of the 2D Vp model.
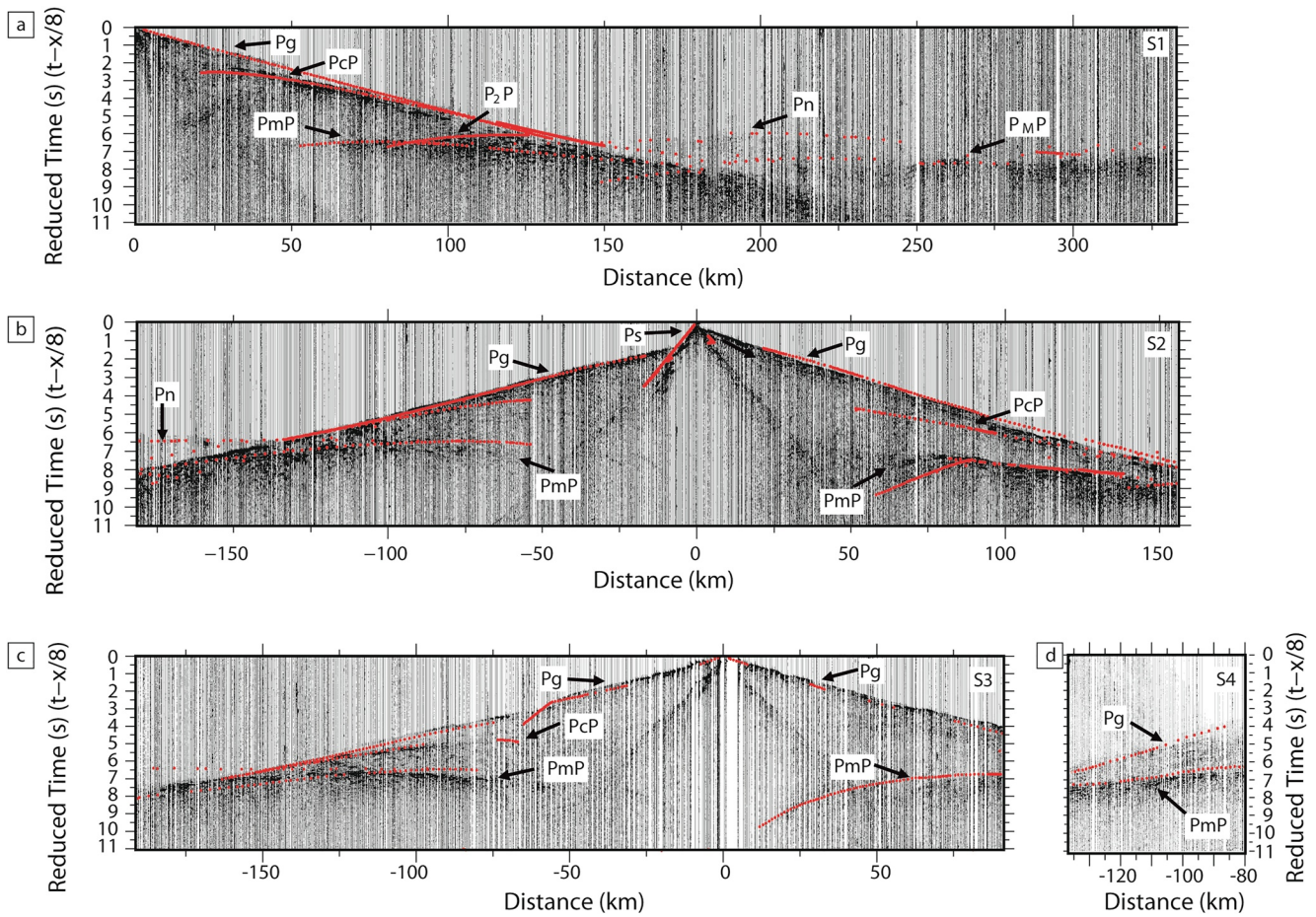
Figure 5. Vertical component record sections from S1 to S4 (same processing flow as applied in Figure 3). Red lines show the theoretical travel-time branches predicted by raytracing through the Vp model shown in Figure 4. Phases are labeled for reference.

The lateral resolution of the model can be estimated by the analysis of the raypath coverage, which reveals the extent to which the different interfaces are constrained by the data. Figure 6 shows examples of the raypath coverage of rays that refract in a layer, rays that reflect off the bottom of a layer and rays that travel as head waves along the bottom of a layer. They are projected over the Vp model for the Cenozoic basins and basement (Figure 6a), lower crust (Figure 6b), and uppermost mantle (Figure 6c). In general, good ray coverage is observed for the Duero Cenozoic basin and SPCS in the crust and upper mantle. However, in the southern end of the profile, the ray coverage is poorer, owing to the limited offset of shot record S4 (Figure 2) and therefore, this part lacks good resolution.

5. Discussion

5.1. Tectonic Model for the Gredos Sector of the SPCS and Its Cenozoic Foreland Basins

The presented Vp model has provided new constraints on the lithospheric structure of the central part of the SPCS and its foreland basins (Figure 7). This part of the SPCS is modeled as a crustal-scale asymmetric thick-skinned double-vergent belt, based on the contrasting image that the Moho boundary reflection (PmP phase; Figure 3b) shows. This phase features opposed dips at similar offsets to the south and north of the SPCS. According to this interpretation, the crustal asymmetry implies that the Gredos sector was, at least, partly exhumed by a system of south-vergent thrusts that imbricate the crust and offset the Moho. Similarly, a magnetotelluric profile crossing the Gredos sector (Pous et al., 2012) revealed zones of relatively high conductivity interpreted as Alpine faults affecting only the upper crust. Nevertheless, the existence of these conductive areas that extends deep in the crust may support the presence of crustal-scale structures.
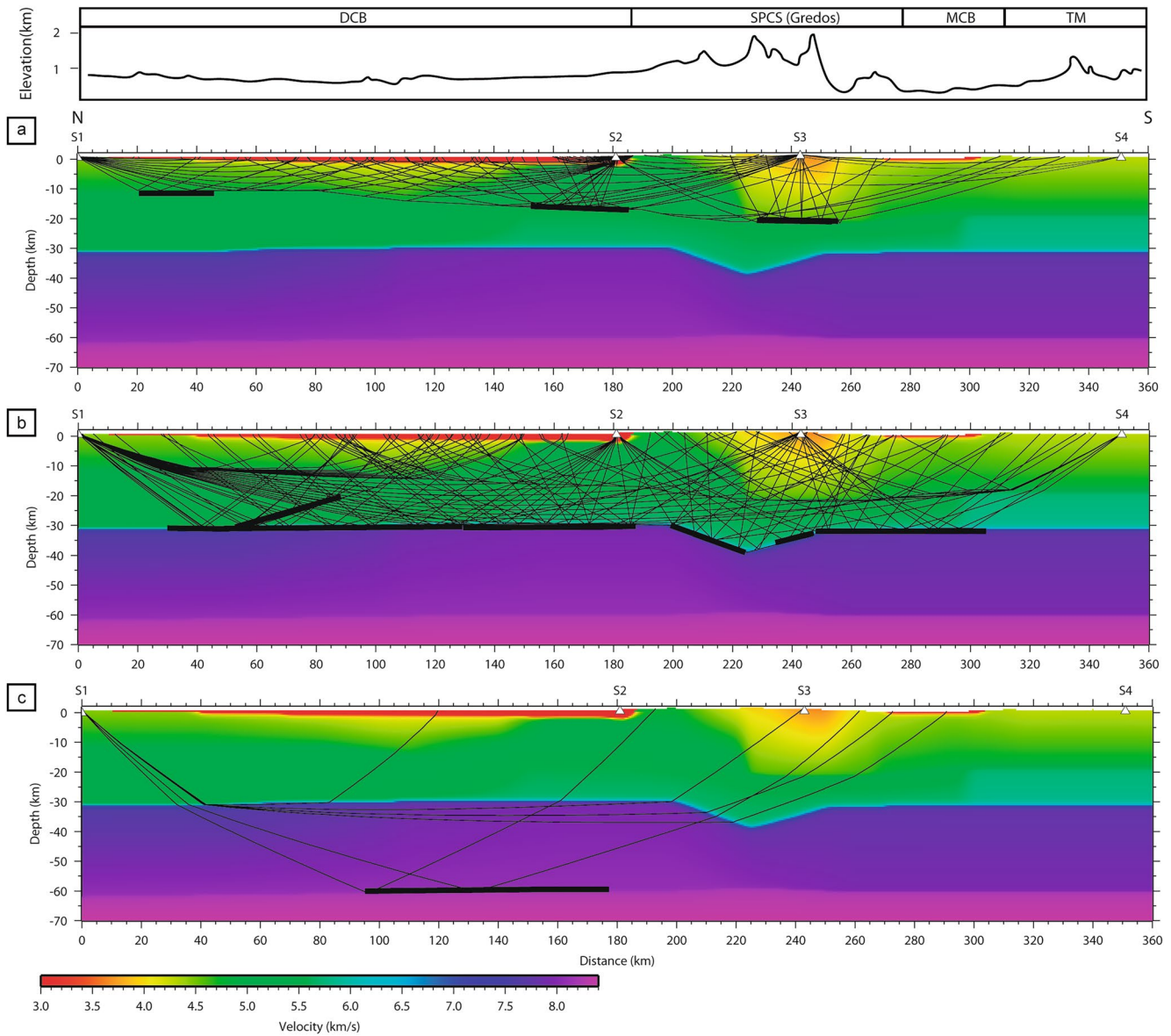
Figure 6. Raypath coverage providing constraints on the lithospheric model determined for the study transect (every tenth ray has been plotted). Rays are projected over the Vp model to provide an idea of the best constrained part of the: (a) upper crust, (b) lower crust, and (c) upper mantle. Bold lines show the interface segments constrained by the data. DCB, Duero Cenozoic basin; MCB, Madrid Cenozoic basin; SPCS, Spanish-Portuguese Central System; TM, Toledo Mountains. S1 to S4 are the sources.

Regarding the crustal geometry, a major north-dipping thrust system would run through the southern border of the dome-shaped iso-velocity contours, representing the Central System batholith, and projecting onto the Tiétar thrust (TiT) system at surface. A second fault system, represented by the South Gredos thrust (SGT), would merge into a mid-crustal detachment or into the TiT system at depth. The role of the SGT is probably more relevant than that of the TiT in the Alpine configuration of the SPCS. Nevertheless, since the SGT is only identified to the east of the CIMDEF profile, where the mountain chain changes its strike from ENE-WSW to NE-SW, its interpretation in our data set and the corresponding Vp model is not straightforward. The exhumation of the SPCS probably resulted from the imbrication of the entire crust in the hanging wall of the south-vergent thrust systems, TiT and SGT. The geometry and activity of these faults may have forced the upper crust south of the Gredos sector to slightly underthrust. These thrust systems, or at least the TiT, failed to root into a missing mid-crustal discontinuity in contrast with the structure of the Cantabrian Mountains, where a mid-crustal detachment enhanced mountain building (Ayarza et al., 2021; Gallastegui et al., 2016; Pulgar et al., 1996).
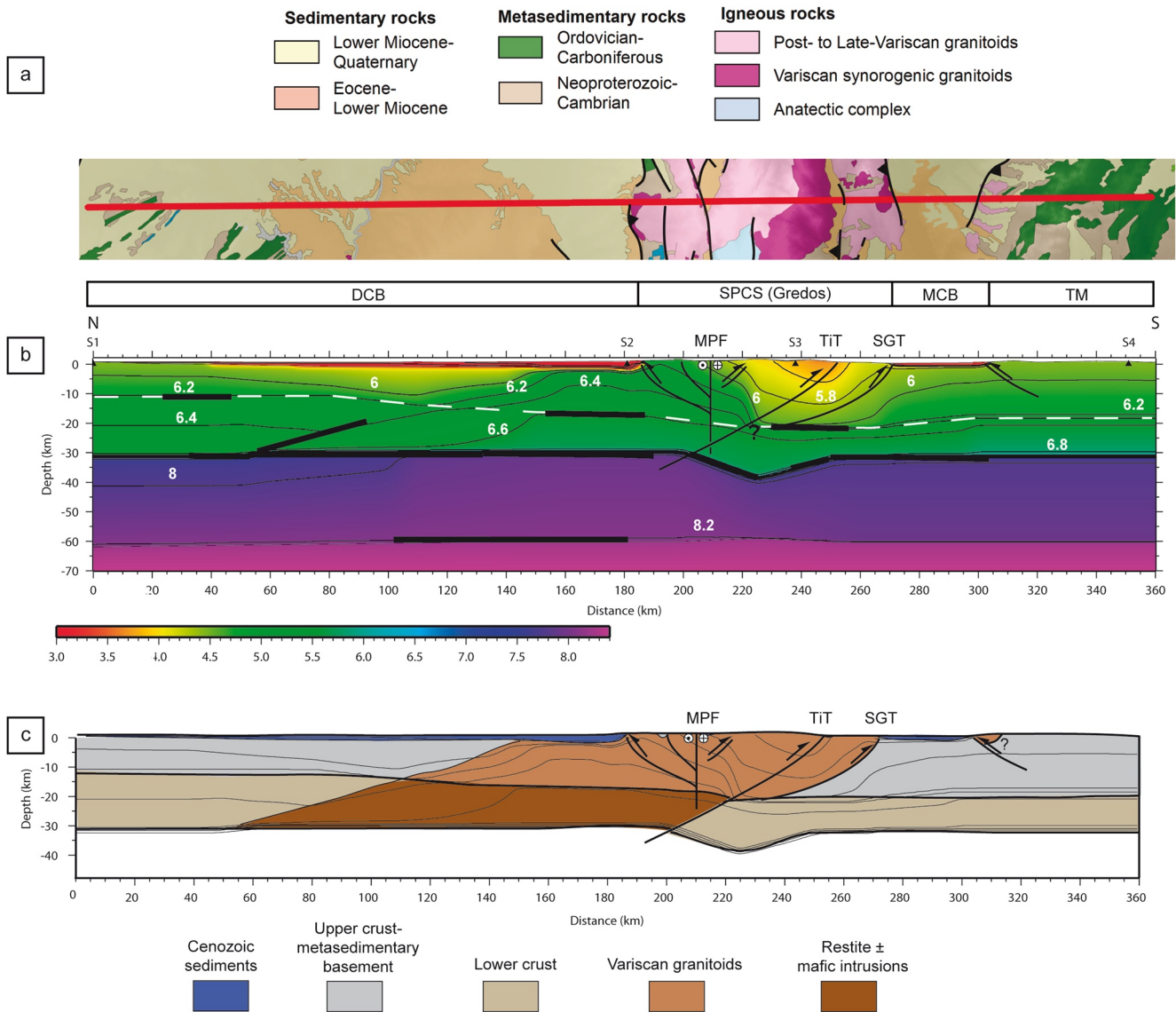
Figure 7. (a) Simplified geological map along the study transect; (b) interpreted Vp model. The thick black lines indicate the location of the top of the lower crust, the internal lower crust reflector, the Moho discontinuity, and the Hales discontinuity constrained by the data and the broken white line the modeled position of the Conrad discontinuity. The main faults (Messejana-Plasencia fault [MPF]; Tiétar thrust [TiT]; and South Gredos thrust [SGT]) and other minor faults are also indicated in the Vp model. DCB, Duero Cenozoic basin; MCB, Madrid Cenozoic basin; SPCS, Spanish-Portuguese Central System; TM, Toledo Mountains; (c) tectonic interpretation of the Vp model. The iso-velocity contours are projected for reference. S1 to S4 are the sources.

Another major fault in the study area corresponds to the NE-SW oriented Messejana-Plasencia fault, assumed to cut the entire crust, and that acted during the Alpine contraction as a left-lateral strike-slip fault. Strain partitioning between the Messejana-Plasencia fault and the main NE-SW oriented faults has been proposed to accommodate the N-S Pyrenean compression (de Vicente et al., 2018). Thus, the mafic rocks associated with the Messejana-Plasencia dyke (Cebriá et al., 2003) might have contributed to the Vp configuration observed to the north of the Gredos sector. However, the dimensions of this structure are below the resolution of the design of this experiment. The Vp model indicates that the Central System batholith may reach a depth of ~19 km under the northern part of the SPCS and most probably also in the southernmost Duero Cenozoic basin. The increase of Vp in the lower crust in that part of the profile may indicate the existence of a significant mafic component in this crustal level, which can be related to high-grade metamorphic rocks, mafic intrusions and/or restite, formed after melt extraction of granite. In the southern part of the SPCS, a decrease of the Vp in the upper crust can be
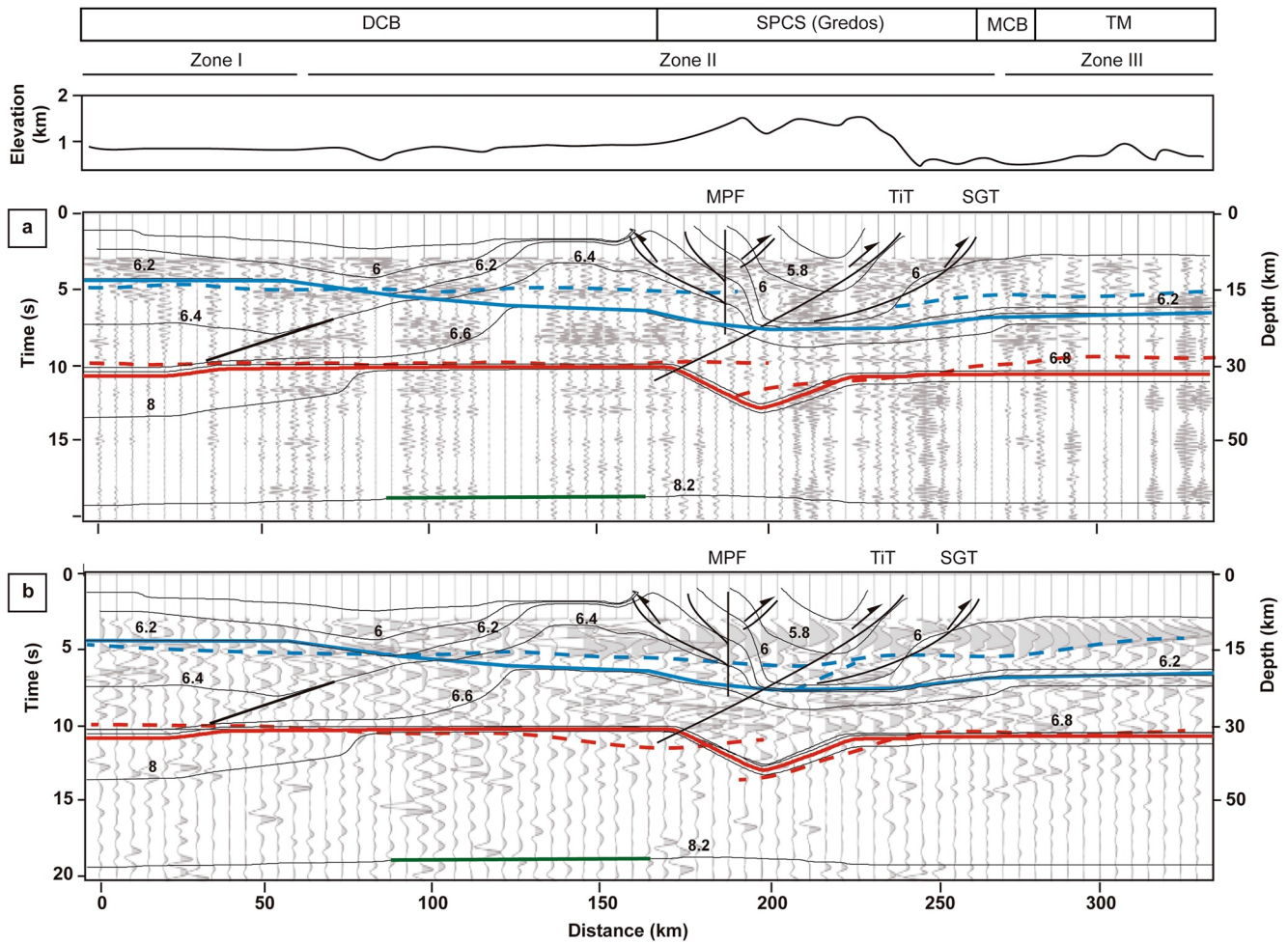
Figure 8. Projection of: (i) our Vp model's iso-velocity contours with numbers indicating the velocity in km/s, (ii) the Conrad discontinuity (blue line), (iii) the Moho discontinuity (red line), (iv) the Hales discontinuity (green line), (v) the interface in the lower crust (black line), and (vi) the main faults in the SPCS Tiétar and South Gredos thrust systems (TiT and SGT) and Messejana-Plasencia fault (MPF) over the lithospheric reflectivity profiles retrieved by: (a) autocorrelation of ambient seismic noise (Andrés et al., 2020, original figure under CC BY 4.0 license); and (b) global-phase seismic interferometry (Andrés et al., 2019, original figure under CC BY 4.0 license). Dashed blue lines represent the top of the lower crust and dashed red lines the Moho discontinuity interpreted by natural source seismic methods. In the upper part, the topography along the natural source transect is shown (Andrés et al., 2019, 2020). DCB, Duero Cenozoic basin; MCB, Madrid Cenozoic basin; SPCS, Spanish-Portuguese Central System; TM, Toledo Mountains.

explained by the upper crust anatexis without much involvement of the lower crust during the late-Variscan deformation. This Vp distribution may not have been significantly affected by the Alpine contraction.

Our model complements previous lithospheric models based on natural source seismic experiments. Figure 8 shows the projection of our iso-velocity contours over the lithospheric reflectivity profiles obtained from seismic noise (Figure 8a) and global-phase seismic interferometry (Figure 8b) as part of the CIMDEF project (Andrés et al., 2019, 2020). The geometry of the Moho discontinuity modeled by both natural and controlled source experiments correlates well, especially with that constrained by global-phase seismic interferometry. Regarding the geometry of the upper-lower crust boundary, despite small mismatches, a general correlation exists under the Duero Cenozoic basin and the Gredos sector. However, toward the south of the profile, we propose a thinner and deeper lower crust than the one interpreted by natural source methods, although our model is less well constrained in the southern region (Figure 6). The model obtained by autocorrelation of seismic noise shows an area of low frequency and high reflectivity under the SPCS which has been interpreted as the Central System batholith (Andrés et al., 2020). This area also coincides with low Vp, reinforcing the same interpretation. Regarding the lower crust, the high frequency and high amplitude reflections found to the north of the SPCS by natural

source methods coincide with the lower part of the dome-shaped distribution of high Vp identified in this work (Figure 8).

5.2. The Conrad Discontinuity: The Upper-Lower Crust Boundary

The data presented in this study show only one intra-crustal phase: PcP (Figure 3). However, this phase is not identified in all the shot records, thus revealing a laterally heterogeneous or elusive character of its source, the Conrad discontinuity.

Based on normal incidence and WA seismic reflection data acquired along the Iberian Massif, one orogen-scale conspicuous mid-crustal feature has been identified and related to the Conrad discontinuity (Ayarza et al., 2021). This boundary might have often acted as a detachment level during the Variscan deformation but also during the Alpine contraction, given the contrasting reflectivity patterns existing between the upper and the lower crust. Along the CIMDEF profile, the Conrad discontinuity, where constraint by the data (Figure 7b), features a Vp contrast of: (a) 6.2–6.3 km/s under the northern Duero Cenozoic basin, (b) 6.5–6.6 km/s under the southern Duero Cenozoic basin, and (c) 6.0–6.5 km/s under the southern part of Gredos. In addition, in the southern part of Gredos, abundant granitoids are modeled as a low Vp area down to 19 km. Thus, the base of Central System batholith seems to extend below the expected position of the Conrad discontinuity, although this boundary shows an irregular or discontinuous character. Accordingly, the lower crust thinned from ∼20 km under the Duero Cenozoic basin to 10–12 km thick under the southern part of Gredos. This velocity pattern may then support a model in which the Conrad discontinuity was partially melted and redefined at the end of the Variscan orogeny. This process might have affected the lower crust, without a significant mantle source and would have kept the Moho flat (Block & Royden, 1990). Although a mantle source in the magmatism of the CIZ is possible, there is no indication of massive mantle participation (Villaseca & Herreros, 2000) as olivine-bearing gabbro is scarce in Gredos (Orejana et al., 2009). Therefore, extension and lateral magma flow may have affected the lower crust. Analog models of continental rifting show that magma and ductile materials in the lower crust are transferred laterally and parallel to the extension direction until they reach a region of lower local pressure and accumulate in the footwall of major faults (Corti et al., 2004). Similarly, in the CIZ the magma flow may have been driven by thinning during extension of a ductile lower crust and by intrusion of crustal melts beneath the area of greatest upper crustal thinning.

In a basement intruded by a huge volume of granitoids (Zone II), the igneous intrusion caused anatexis of the crust, interrupting or even assimilating a mid-crustal detachment horizon in which the Alpine thrusts could have soled out. Thus, the upper-lower crust boundary was partly obliterated and redefined after cooling, leading to an irregular discontinuity sampled as the PcP phase in our data set. Therefore, the TiT (Figure 7) did not find a major mid-crustal detachment to root in and instead might have followed the southern Central System batholith affecting the entire crust. Additionally, the SGT, which plays a key role in the exhumation of the Gredos sector to the east, could have either rooted at the mid-crustal detachment or joined the TiT at depth. This pattern is not observed in other ranges formed in the borders of the Iberian microplate, that is, the Cantabrian Mountains, where Teixell et al. (2018) proposed the preservation of the mid-crustal detachment allowed for underthrusting of the lower crust. Accordingly, we suggest that the crustal structure and deformation mechanisms affecting Gredos during the Alpine contraction are significantly controlled by the inferred volume of granitoids at depth, playing a role in the nucleation of the SPCS (de Vicente et al., 2018), and enhancing coupled Alpine deformation between the upper and lower crust (Ayarza et al., 2021).

5.3. The Moho Discontinuity

The crust-mantle boundary is essentially flat in the Iberian Massif except when there are remnants of Variscan imbrications or it is affected by the Alpine contraction (Ayarza et al., 2021; Martínez Poyatos et al., 2012; Simancas et al., 2013). A generally flat subhorizontal Moho is identified at depths of 31–33 km (Ehsan et al., 2014; Palomeras et al., 2009; Palomeras, Ehsan, et al., 2021) in the southern CIZ, Ossa-Morena zone, and South Portuguese zone. However, under the SPCS, the accommodation of the crustal compression during the Alpine contraction resulted in a Moho offset from ∼33 to 39 km depth along 25 km. A Moho depth of 40 km was also obtained by potential field (gravity and geoid) modeling and thermal analysis (Torne et al., 2015) and natural source seismic experiments (Andrés et al., 2019, 2020) (Figure 8). This Moho geometry is compatible

with an imbrication of the crust and incipient continental subduction in the southern part of the CIZ under the Gredos sector after the development of south-vergent thrust systems (de Vicente et al., 2021). The contrasting geometry of the PmP phase in S2 (Figure 3b) to the north (relatively flat between −130-km and −40-km offset) and south (north-dipping at 50-km to 160-km offset) of the SPCS also confirm the asymmetric crustal geometry as a crustal-scale pop-up (de Vicente et al., 2018), and a thickening of the crust under the SPCS (Vegas & Suriñach, 1987).

5.4. The Hales Discontinuity

The reflector modeled from the conspicuous subcrustal feature, P_MP (Figure 3a), coincides with the depth and character proposed for the Hales discontinuity, a mineral phase transition from spinel-lherzolite to garnet-lherzolite in the upper mantle. The top of this reflection is located at 59–60 km under the southern border of the Duero Cenozoic basin. As it has only been imaged in S1, its continuation toward the south (∼180-km offset) is uncertain (Figure 6c).

In the Central Iberian, Ossa-Morena, and South Portuguese zones (Figure 1), subcrustal sub-horizontal reflections have been identified in deep seismic sounding experiments. Along the ALCUDIA-NI profile (Martínez Poyatos et al., 2012), an outstanding subcrustal reflection is identified at 19 s twtt (∼57 km) in the central part of the CIZ and at 16 s twtt (∼48 km) in its southern part. New processing and modeling along the ALCUDIA-WA and ILIHA profiles (see location in Figure 1b) located such discontinuity at 51–57 km under the southern part of the CIZ and SPCS (Palomeras, Ayarza, et al., 2021). Additionally, the Hales discontinuity has been described in the IBERSEIS-WA profile as a gradient zone located at 61–72 km, and with a Vp contrast from 8.2 to 8.3 km/s (Ayarza et al., 2010).

The depth of the Hales discontinuity depends on the mantle geochemistry, but it can be generally placed at ∼65 km depending on mantle depletion (O'Neill, 1981). In addition, a gradual conversion from spinel to garnet may explain the characteristics of the reflections coming off this boundary (high amplitude and long coda), pointing to some sort of complexity (i.e., layering where the amount of spinel with respect to garnet is variable, Ayarza et al., 2010; Palomeras, Ayarza, et al., 2021), thus producing constructive seismic interferences. Regardless of only being imaged in one of the shots, the data set presented here contains one of the best recorded reflections of the so-called Hales discontinuity (P_MP in Figure 3a). Its high amplitude and lateral continuity allow defining its smooth sub-horizontal geometry which does not seem to have been affected by the Alpine contraction. Therefore, our data suggest that the Alpine contraction affected only the crust, offsetting the Moho (as revealed by the asymmetry of the PmP phases), but preserving lithospheric mantle features.

5.5. The Variscan Orogeny in the CIZ

Although our Vp model provides information about the lithospheric structure of an Alpine intraplate range, this tectonic configuration has been influenced by the evolution during the Variscan orogeny.

The Variscan orogeny led to crustal thickening during the early Carboniferous, before its late-Variscan thermal weakening and gravitational collapse (Barbero & Villaseca, 2000; Rubio Pascual et al., 2013, 2016). In some places of the CIZ, the lower crust was significantly thinned by pervasive extension and widespread melting processes (Alcock et al., 2015; Ayarza et al., 2021; Díez Fernández & Pereira, 2016; Escuder Viruete et al., 1998; Martínez Catalán et al., 2014), also evidenced by the intrusion of late-Variscan granitoids (e.g., Bea et al., 2003; Orejana et al., 2012; Simancas et al., 2013). The generalized gravitational collapse of this orogen and crustal thinning was driven by broad ductile shear zones that formed under a regional N-S to NW-SE direction of extension (e.g., Dias da Silva et al., 2021; Doblas, 1991; Doblas, López-Ruiz, et al., 1994; Escuder Viruete et al., 1998). Associated to these late-Variscan low-angle detachment tectonics and shear zones, uplift of deep and hot rocks in the footwall of these detachments caused a progressive doming of the overlying mylonitic zone resulting in an asymmetric antiform (Doblas, López-Ruiz, et al., 1994; Escuder Viruete et al., 1994). This doming may have been also induced by the granitoid emplacement (Escuder Viruete et al., 2000) and caused an intense anatexis in the CIZ (Díaz Alvarado et al., 2013; Diez Balda et al., 1995; Doblas, Oyarzun, et al., 1994).

Therefore, the intrusion of the Central System granitoids would have melted the host rocks and partially assimilated the mid-crustal detachment, where the Variscan tectonic structures (compressional or extensional) rooted

(or should have rooted). This process may have also enhanced the formation of zones of rheological contrasts where new structures could nucleate to accommodate the deformation during the forthcoming Alpine contraction. In fact, the pop-up and pop-down Alpine structures in the SPCS have been related to the existence of a homogeneous crustal rheology due to the abundance of granite in Gredos (de Vicente & Muñoz-Martín, 2013).

5.6. The Alpine Contraction: Shortening, Deformation Transfer, and Detachment Levels

Major deformation related to the Alpine contraction was concentrated in the Iberian microplate boundaries, mostly within the Pyrenean-Cantabrian mountain chain and the Betic Cordillera (Figure 1b). Thus, the exhumation of the SPCS resulted from the deformation transfer from the Iberian microplate boundaries to the interior (e.g., de Vicente et al., 2018; Fernández-Lozano et al., 2011).

The Alpine collision of the Iberian microplate with the Eurasian plate resulted in an asymmetric crustal architecture and Moho offset under the SPCS. The crustal structure in Figure 7c implies a low shortening, possibly <15 km. However, the modeling strategy carried out in this work does not allow to image layer duplications, hindering the possibility of picturing the entire geometry of the imbrication. In this same area of Gredos, Andrés et al. (2020) provided a shortening of ~20 km. To the east, in Guadarrama, where the existence of an Upper Cretaceous cover allowed for a more precise reconstruction, 24 km of shortening in the upper crust was calculated (de Vicente & Vegas, 2009; Quintana et al., 2015). This difference in the estimated shortening along the SPCS agrees with a thermochronological study that revealed less denudation and rock exhumation in Gredos (De Bruijne & Andriessen, 2002). Furthermore, the amount of ductile deformation, mostly at lower crustal levels, cannot be estimated, hindering precise comparisons between shortening at different crustal levels.

The shortening values estimated for the SPCS contrast with the 90 to >170 km calculated for the Pyrenees-Cantabrian Mountains (DeFelipe et al., 2018; Jammes et al., 2014; Muñoz, 1992; Teixell et al., 2016). There, the development of thick Cretaceous sedimentary basins (North Pyrenean Zone and Basque-Cantabrian basin) in a hyperextended margin where low-angle detachment faults formed (Clerc et al., 2016; DeFelipe et al., 2017, 2019; Masini et al., 2014), as well as Cenozoic syntectonic basins (South Pyrenean Zone; Labaume et al., 2016; Teixell & García-Sansegundo, 1995), conditioned the subsequent tectonic inversion. Regarding the SPCS, where no thick basins formed over the Variscan basement, only ~4 km of vertical movement are predicted (De Bruijne & Andriessen, 2002). From the middle Eocene to the early Miocene, N-S compression related to the Pyrenean-Cantabrian orogen formation was transferred toward the south, inducing compression and exhumation in the Gredos and Guadarrama sectors, as evidenced by low-temperature thermochronological dating (De Bruijne & Andriessen, 2002; Sell et al., 1995). Subsequently, from 9 to 3.7 Ma, the NW-SE compression related to the Betic Cordillera was transferred to the SPCS and produced a limited reactivation of previous structures (de Vicente et al., 2018).

The lithospheric model presented in this work also highlights the influence of the granitoids in the rheological behavior of the crust. Batholiths can behave as highly competent bodies, concentrating deformation in its edges and in adjacent host rocks, thus, partitioning the strain to other domains (Miller & Paterson, 2001). Therefore, fault nucleation is preferentially focused into zones of strong rheological contrast, such as the granite contacts or at the boundaries with the host rocks (D'Lemos et al., 1997). Indeed, the boundary between the SPCS granitoids and the metasedimentary rocks of the CIZ south of Gredos, represents a zone of strong rheological anisotropy. This contrast may have controlled the kinematics of the SGT leading it to skip an elusive and interrupted Conrad discontinuity redefined after the Variscan granite emplacement and offsetting the entire crust. The granitoids not only assimilated the mid-crustal detachment during its late-Variscan emplacement, but also helped to define a new subvertical to north-dipping weakness zone.

Our results therefore support the relevance of the Variscan batholith in the nucleation of the Alpine structures in the SPCS, as it was previously proposed by de Vicente et al. (2018) based on the orientation of the structures. Consequently, the upper crust in the footwall of the TiT and SGT may also have slightly underthrust. This crustal architecture may be partly responsible of the different altitudes between the Duero and Madrid Cenozoic basins (Andrés et al., 2020). In this regard, it is worth noting that both the Duero and Madrid Cenozoic basins experienced a different sedimentation and erosional history during the Cenozoic (Cunha, de Vicente, et al., 2019; Cunha, Martins, et al., 2019; Silva et al., 2017) that could partly explain this difference in altitude. The *Raña surface* represents an extensive alluvial planation landform, present in both Madrid and Duero Cenozoic

basins, that pre-dates the Quaternary fluvial incision (Gutiérrez-Elorza et al., 2002; Karampaglidis et al., 2020; Martín-Serrano, 1991; Pérez-González, 1994). Maximum fluvial incision calculated from this surface implies incision of 220 m for the Madrid Cenozoic basin and 165 m for the Duero Cenozoic basin (Silva et al., 2017). Furthermore, in the Madrid Cenozoic basin and south of the Guadarrama sector, recent and historical seismicity (Rodríguez-Pascua et al., 2016) is explained by Giner-Robles et al. (2012) as: (a) tectonic far-field stress of plate convergence, (b) lithospheric flexion evidenced by large basement wave-length folding, and (c) the tectonic loading associated with the topography of the SPCS. We therefore suggest that the exhumation of the SPCS by south-directed thick-skinned thrusts may be related to the underthrusting of the basement south of the SPCS and be one of the mechanisms responsible for the difference in altitude in both foreland basins influenced by their different erosional history (de Vicente & Muñoz-Martín, 2013).

Finally, our model discards lithospheric folding/buckling (e.g., Cloetingh et al., 2002) as the main deformation mechanism in the SPCS. The crustal structure in the study area results from a complex geological evolution since the Variscan orogeny. The resulting Alpine crustal asymmetry, otherwise similar to that observed in some sections of other Alpine mountain ranges (Alps, Pyrenees, or Cantabrian Mountains), is promoted by a system of thrusts that follow the SPCS southern boundary and affects the upper and lower crust in a fairly coupled way. Thus, the crustal discontinuities and rheological contrasts contributed to the exhumation of the SPCS intraplate mountain range and an incipient and restricted crustal subduction.

6. Conclusions

In this study, we present a lithospheric model of the Gredos sector of the SPCS intraplate mountain range and its foreland Duero and Madrid Cenozoic basins, based on the CIMDEF wide-angle seismic reflection/refraction experiment. The P-wave velocity model obtained shows a layered lithosphere with three main discontinuities: (a) the upper and lower crust boundary, the Conrad discontinuity, is located between 10.5 km depth in the north and 18 km depth in the south; (b) the crust and mantle boundary, the Mohorovicic discontinuity, is relatively flat under the Duero Cenozoic basin and southern part of the profile with an offset from 33 to 39 km under the SPCS; and (c) an upper mantle boundary under the Duero Cenozoic basin, the Hales discontinuity, at 59–60 km depth, which is the most outstanding and continuous reflection of the lithospheric mantle under the Iberian Massif. Our model also suggests the existence of a large batholith coinciding with the dome-shaped iso-velocity contours under the Gredos sector and the southernmost part of the Duero Cenozoic basin. In the southern part of Gredos, a reduction of the P-wave velocity in the upper crust may reflect a change in the lithological variability of the batholith exhumed along the SPCS. Additionally, the lower crust thins toward the south. The interpreted crustal structure consists of two major thick-skinned south-vergent thrust systems: the Tiétar thrust exhumed the SPCS causing a crustal imbrication and a Moho offset, and the South Gredos thrust, sampled close to its termination, which might root in the mid-crustal detachment or locally merged the Tiétar thrust at depth.

During the gravitational collapse of the Variscan orogen in the late Carboniferous, pervasive extension and melting in the CIZ triggered the intrusion of granitoids in the present-day Gredos sector. These granitoids most probably derive from anatexis of upper crust levels and therefore, do not affect much of the lower crust, which may be formed by restite, mafic intrusions (if a mantle source was involved) and/or high-grade metamorphic rocks. Late-Variscan detachment faults and shear zones formed and rooted in a mid-crustal detachment where it was not assimilated by the SPCS basement granitoids. However, close to this mountain range, a large part of this detachment might have been erased or reworked, changing the rheology of the crust and defining new weak zones that would be preferentially used by contractional Alpine structures, such as the southern border of the SPCS. In this context, the Alpine contraction, which resulted in the exhumation of the Pyrenean-Cantabrian Mountain belt in the northern border of the Iberian microplate, was also transferred to the plate's interior exhuming the Neoroterozoic-Paleozoic rocks of the SPCS since the Eocene with a low shortening rate despite its high topography.

Our lithospheric model has major implications into the crustal deformation mechanisms. The granitoids of the basement of the SPCS not only assimilated the mid-crustal detachment horizon but also defined a new weak zone that controlled the nucleation of the crustal-scale Alpine thrust systems. Consequently, the upper crust in the footwall of the Tiétar and South Gredos thrust systems may also have slightly underthrust. The origin of the noteworthy topography difference between the Madrid and Duero Cenozoic basins could be related to the afore-

mentioned tectonic mechanisms as well as slightly influenced by the different erosional history in the basins, opening a line of research for future work in this matter.

This work has provided a new lithospheric model of an intraplate mountain range, showing that pre-Alpine crustal discontinuities and rheological contrasts enhanced intraplate mountain building during the Alpine contraction.

Data Availability Statement

Data are available online in the SeisDARE database (https://digital.csic.es/handle/10261/101879, last accessed May 2022) (DeFelipe et al., 2021). The shot records are available in Ayarza and Carbonell (2019).

References

Álvaro, J. J., & Lorenzo, S. (2021). Cadomian orogenic collapse in the Ibor and Alcudia anticlines of the Central Iberian Zone, Spain. *Geological Magazine*, 1–11. https://doi.org/10.1017/S0016756821000339

Aitken, A. R. A., Raimondo, T., & Capitanio, F. A. (2013). The intraplate character of supercontinent tectonics. *Gondwana Research*, *24*(3–4), 807–814. https://doi.org/10.1016/j.gr.2013.03.005

Alcock, J. E., Martínez Catalán, J. R., Catalán, M., Francisco, J., Pascual, R., Montes, A. D., et al. (2015). 2-D thermal modeling of HT–LP metamorphism in NW and Central Iberia: Implications for Variscan magmatism, rheology of the lithosphere and orogenic evolution. *Tectonophysics*, *657*, 21–37. https://doi.org/10.1016/j.tecto.2015.05.022

Alonso, A., Floquet, M., Mas, R., & Meléndez, A. (1993). Late Cretaceous Platforms: Origin and evolution, Iberian Range, Spain. *AAPG Special*, *56*, 297–313.

Andrés, J., Ayarza, P., Schimmel, M., Palomeras, I., Ruiz, M., & Carbonell, R. (2020). What can seismic noise tell us about the Alpine reactivation of the Iberian Massif? An example in the Iberian Central System. *Solid Earth*, *11*, 2499–2513. https://doi.org/10.5194/se-11-2499-2020

Andrés, J., Draganov, D., Schimmel, M., Ayarza, P., Palomeras, I., Ruiz, M., & Carbonell, R. (2019). Lithospheric image of the Central Iberian Zone (Iberian Massif) using global-phase seismic interferometry. *Solid Earth*, *10*(6), 1937–1950. https://doi.org/10.5194/se-10-1937-2019

Arenas, R., Sánchez Martínez, S., Gerdes, A., Albert, R., Díez Fernández, R., & Andonaegui, P. (2014). Re-interpreting the Devonian ophiolites involved in the Variscan suture: U-Pb and Lu-Hf zircon data of the Moeche Ophiolite (Cabo Ortegal Complex, NW Iberia). *International Journal of Earth Sciences*, *103*(5), 1385–1402. https://doi.org/10.1007/s00531-013-0880-x

Ayarza, P., & Carbonell, R. (2019). CIMDEF: A wide-angle deep seismic reflection profile in the Central Iberian Zone. [Data Set]. https://doi.org/10.20350/digitalCSIC/10528

Ayarza, P., Martínez Catalán, J. R., Martínez García, A., Alcalde, J., Andrés, J., Simancas, J. F., et al. (2021). Evolution of the Iberian Massif as deduced from its crustal thickness and geometry of a mid-crustal (Conrad) discontinuity. *Solid Earth*, *12*, 1515–1547. https://doi.org/10.5194/se-12-1515-2021

Ayarza, P., Palomeras, I., Carbonell, R., Afonso, J. C., & Simancas, F. (2010). A wide-angle upper mantle reflector in SW Iberia: Some constraints on its nature. *Physics of the Earth and Planetary Interiors*, *181*(3–4), 88–102. https://doi.org/10.1016/j.pepi.2010.05.004

Azor, A., Dias da Silva, Í., Gómez Barreiro, J., González-Clavijo, E., Martínez Catalán, J. R., Simancas, J. F., et al. (2019). Deformation and structure. In *The geology of Iberia: A geodynamic approach* (pp. 307–348). Cham: Springer. https://doi.org/10.1007/978-3-030-10519-8_10

Banda, E., Suriñach, E., Aparicio, A., Sierra, J., & Ruiz de la Parte, E. (1981). Crust and upper mantle structure of the central Iberian Meseta (Spain). *Geophysical Journal International*, *67*, 779–789. https://doi.org/10.1111/j.1365-246x.1981.tb06954.x

Bandrés, A., Eguíluz, L., Pin, C., Paquette, J. L., Ordóñez, B., Le Fèvre, B., et al. (2004). The northern Ossa-Morena Cadomian batholith (Iberian Massif): Magmatic arc origin and early evolution. *International Journal of Earth Sciences*, *93*(5), 860–885. https://doi.org/10.1007/s00531-004-0423-6

Barbero, L., & Villaseca, C. (2000). Eclogite facies relics in metabasites from the Sierra de Guadarrama (Spanish Central System): P-T estimations and implications for the Hercynian evolution. *Mineralogical Magazine*, *64*, 815–836. https://doi.org/10.1180/002646100549814

Bea, F. (1985). Los granitoides hercínicos de la mitad Occidental del Batolito de Avila (Sector de Gredos): Aproximación mediante el concepto de superfacies. *Rev. Real. Acad. Cien. Fis. Exac. Nat. Madrid*, *79*, 549–572.

Bea, F., Montero, P., & Molina, J. F. (1999). Mafic precursors, peraluminous granitoids, and late lamprophyres in the Avila batholith: A model for the generation of Variscan batholiths in Iberia. *The Journal of Geology*, *107*(4), 399–419. https://doi.org/10.1086/314356

Bea, F., Montero, P., & Zinger, T. (2003). The nature, origin, and thermal influence of the granite source layer of Central Iberia. *The Journal of Geology*, *111*(5), 579–595. https://doi.org/10.1086/376767

Bea, F., Montero, P. G., González-Lodeiro, F., Talavera, C., Molina, J. F., Scarrow, J. H., et al. (2006). Zircon thermometry and U-Pb ion-microprobe dating of the gabbros and associated migmatites of the Variscan Toledo Anatectic Complex, Central Iberia. *Journal of the Geological Society*, *163*, 847–855. https://doi.org/10.1144/0016-76492005-143

Bea, F., & Pereira, M. D. (1990). Estudio petrológico del Complejo Anatéctico de la Peña Negra (batolitlo de Ávila, España Central). *Revista de la Sociedad Geologica de Espana*, *3*(1–2), 87–105.

Birch, F. (1960). The velocity of compressional waves in rocks to 10 kilobars: 1. *Journal of Geophysical Research (1896-1977)*, *65*(4), 1083–1102. https://doi.org/10.1029/JZ065i004p01083

Block, L., & Royden, L. H. (1990). Core complex geometries and regional scale flow in the lower crust. *Tectonics*, *9*(4), 557–567. https://doi.org/10.1029/tc009i004p00557

Brown, D., Carbonell, R., Kukkonen, I., Ayala, C., & Golovanova, I. (2003). Composition of the Uralide crust from seismic velocity (Vp, Vs), heat flow, gravity, and magnetic data. *Earth and Planetary Science Letters*, *210*(1–2), 333–349. https://doi.org/10.1016/S0012-821X(03)00143-2

Cadenas, P., & Fernández-Viejo, G. (2017). The Asturian Basin within the North Iberian margin (Bay of Biscay): Seismic characterisation of its geometry and its Mesozoic and Cenozoic cover. *Basin Research*, *29*(4), 521–541. https://doi.org/10.1111/bre.12187

Cambeses, A., Scarrow, J. H., Montero, P., Lázaro, C., & Bea, F. (2016). Palaeogeography and crustal evolution of the Ossa–Morena Zone, southwest Iberia, and the North Gondwana margin during the Cambro-Ordovician: A review of isotopic evidence. *International Geology Review*, *59*(1), 94–130. https://doi.org/10.1080/00206814.2016.1219279

Casas-Sainz, A. M., & de Vicente, G. (2009). On the tectonic origin of Iberian topography. *Tectonophysics*, *474*(1–2), 214–235. https://doi.org/10.1016/j.tecto.2009.01.030

Castiñeiras, P., Villaseca, C., Barbero, L., & Romera, M. C. (2008). SHRIMP U-Pb zircon dating of anatexis in high-grade migmatite complexes of Central Spain: Implications in the Hercynian evolution of Central Iberia. *International Journal of Earth Sciences*, *97*(1), 35–50. https://doi.org/10.1007/s00531-006-0167-6

Cebriá, J. M., López-Ruiz, J., Doblas, M., Martins, L. T., & Munha, J. (2003). Geochemistry of the early Jurassic Messejana- Plasencia dyke (Portugal-Spain): Implications on the origin of the Central Atlantic magmatic province. *Journal of Petrology*, *44*(3), 547–568. https://doi.org/10.1093/petrology/44.3.547

Chappell, B. W., White, A. J. R., & Wyborn, D. (1987). The importance of residual source material (restite) in granite petrogenesis. *Journal of Petrology*, *28*(6), 1111–1138. https://doi.org/10.1093/petrology/28.6.1111

Chroston, P. N., & Evans, C. J. (1983). Seismic velocities of granulites from the Seiland Petrographic Province, N Norway: Implications for Scandinavian lower continental crust. *Journal of Geophysics - Zeitschrift Fur Geophysik*, *52*(1), 14–21.

Clerc, C., Lagabrielle, Y., Labaume, P., Ringenbach, J. C., Vauchez, A., Nalpas, T., et al. (2016). Basement – Cover decoupling and progressive exhumation of metamorphic sediments at hot rifted margin. Insights from the Northeastern Pyrenean analog. *Tectonophysics*, *686*, 82–97. https://doi.org/10.1016/j.tecto.2016.07.022

Cloetingh, S., Burov, E., Beekman, F., Andeweg, B., Andriessen, P. A. M., Garcia-Castellanos, D., et al. (2002). Lithospheric folding in Iberia. *Tectonics*, *21*(5), 5-1–5–26. https://doi.org/10.1029/2001TC901031

Corti, G., Bonini, M., Sokoutis, D., Innocenti, F., Manetti, P., Cloetingh, S., & Mulugeta, G. (2004). Continental rift architecture and patterns of magma migration: A dynamic analysis based on centrifuge models. *Tectonics*, *23*(2). https://doi.org/10.1029/2003TC001561

Cunha, P. P., de Vicente, G., & Martín-González, F. (2019). *Cenozoic sedimentation along the piedmonts of thrust related basement ranges and strike-slip deformation belts of the Iberian Variscan Massif*. Springer International Publishing. https://doi.org/10.1007/978-3-030-11190-8_5

Cunha, P. P., Martins, A. A., Gomes, A., Stokes, M., Cabral, J., Lopes, F. C., et al. (2019). Mechanisms and age estimates of continental-scale endorheic to exorheic drainage transition: Douro River, Western Iberia. *Global and Planetary Change*, *181*, 102985. https://doi.org/10.1016/j.gloplacha.2019.102985

D'Lemos, R. S., Schofield, D. I., Holdsworth, R. E., & King, T. R. (1997). Deep crustal and local rheological controls on the siting and reactivation of fault and shear zones, northeastern Newfoundland. *Journal of the Geological Society*, *154*(1), 117–121. https://doi.org/10.1144/gsjgs.154.1.0117

Dallmeyer, R. D., Martínez Catalán, J. R., Arenas, R., Gil Ibarguchi, J. I., Gutiérrez-Alonso, G., Farias, P., et al. (1997). Diachronous Variscan tectonothermal activity in th NW Iberia Massif: Evidence from 40Ar/39Ar dating of regional fabrics. *Tectonophysics*, *277*(4), 307–337. https://doi.org/10.1016/s0040-1951(97)00035-8

de Vicente, G., Cunha, P. P., Muñoz-Martín, A., Cloetingh, S. A. P. L., Olaiz, A., & Vegas, R. (2018). The Spanish-Portuguese Central System: An example of intense intraplate deformation and strain partitioning. *Tectonics*, *37*(12), 4444–4469. https://doi.org/10.1029/2018TC005204

de Vicente, G., & Muñoz-Martín, A. (2013). The Madrid Basin and the Central System: A tectonostratigraphic analysis from 2D seismic lines. *Tectonophysics*, *602*, 259–285. https://doi.org/10.1016/j.tecto.2012.04.003

de Vicente, G., Olaiz, A., Muñoz-Martín, A., & Cunha, P. P. (2021). Longest and still longer: The Messejana-Plasencia dyke and its links with later Alpine deformation belt in Iberia. *Tectonophysics*, *815*, 229009. https://doi.org/10.1016/j.tecto.2021.229009

de Vicente, G., & Vegas, R. (2009). Large-scale distributed deformation controlled topography along the Western Africa-Eurasia limit: Tectonic constraints. *Tectonophysics*, *474*(1–2), 124–143. https://doi.org/10.1016/j.tecto.2008.11.026

de Vicente, G., Vegas, R., Muñoz Martín, A., Silva, P. G., Andriessen, P., Cloetingh, S., et al. (2007). Cenozoic thick-skinned deformation and topography evolution of the Spanish Central System. *Global and Planetary Change*, *58*(1–4), 335–381. https://doi.org/10.1016/j.gloplacha.2006.11.042

De Bruijne, C. H., & Andriessen, P. A. M. (2002). Far field effects of Alpine plate tectonism in the Iberian microplate recorded by fault-related denudation in the Spanish Central System. *Tectonophysics*, *349*(1–4), 161–184. https://doi.org/10.1016/S0040-1951(02)00052-5

DeFelipe, I., Alcalde, J., Ivandic, M., Martí, D., Ruiz, M., Marzán, I., et al. (2021). Reassessing the lithosphere: SeisDARE, an open access seismic data repository. *Earth System Science Data*, *13*, 1053–1071. https://doi.org/10.5194/essd-13-1053-2021

DeFelipe, I., Pedreira, D., Pulgar, J. A., Iriarte, E., & Mendia, M. (2017). Mantle exhumation and metamorphism in the Basque-Cantabrian Basin (N Spain): Stable and clumped isotope analysis in carbonates and comparison with ophicalcites in the North-Pyrenean Zone (Urdach and Lherz). *Geochemistry, Geophysics, Geosystems*, *18*(2), 631–632. https://doi.org/10.1002/2016GC006690

DeFelipe, I., Pedreira, D., Pulgar, J. A., van der Beek, P. A., Bernet, M., & Pik, R. (2019). Unraveling the mesozoic and cenozoic tectonothermal evolution of the Eastern Basque-Cantabrian Zone–Western Pyrenees by low-temperature thermochronology. *Tectonics*, *38*(9), 3436–3461. https://doi.org/10.1029/2019TC005532

DeFelipe, I., Pulgar, J. A., & Pedreira, D. (2018). Crustal structure of the eastern Basque-Cantabrian zone – Western Pyrenees: From the Cretaceous hyperextension to the Cenozoic inversion. *Revista de la Sociedad Geologica de Espana*, *31*(2), 69–82. https://sge.usal.es/archivos/REV/31(2)/RSGE31(2)_p_69_82.pdf

De Vicente, G., Cloetingh, S., Van Wees, J. D., & Cunha, P. P. (2011). Tectonic classification of Cenozoic Iberian foreland basins. *Tectonophysics*, *502*(1–2), 38–61. https://doi.org/10.1016/j.tecto.2011.02.007

De Vicente, G., Giner, J. L., Muñoz-Martí, A., González-Casado, J. M., & Lindo, R. (1996). Determination of present-day stress tensor and neotectonic interval in the Spanish Central System and Madrid Basin, central Spain. *Tectonophysics*, *266*(1–4), 405–424. https://doi.org/10.1016/S0040-1951(96)00200-4

Dewey, J. F., & Bird, J. M. (1970). Mountain belts and the new global tectonics. *Journal of Geophysical Research (1896-1977)*, *75*(14), 2625–2647. https://doi.org/10.1029/JB075i014p02625

Dias da Silva, Í., González Clavijo, E., & Díez-Montes, A. (2021). The collapse of the Variscan belt: A Variscan lateral extrusion thin-skinned structure in NW Iberia. *International Geology Review*, *63*(6), 659–695. https://doi.org/10.1080/00206814.2020.1719544

Díaz, J., DeFelipe, I., Ruiz, M., Andrés, J., Ayarza, P., & Carbonell, R. (2022). Identification of natural and anthropogenic signals in controlled source seismic experiments. *Scientific Reports*, *12*, 3171. https://doi.org/10.1038/s41598-022-07028-3

Díaz, J., Gallart, J., Córdoba, D., Senos, L., Matias, L., Suriñach, E., et al. (1993). A deep seismic sounding investigation of lithospheric heterogeneity and anisotropy beneath the Iberian Peninsula. *Tectonophysics*, *221*(1), 35–51. https://doi.org/10.1016/0040-1951(93)90026-G

Díaz Alvarado, J., Fernández, C., Castro, A., & Moreno-Ventas, I. (2013). SHRIMP U–Pb zircon geochronology and thermal modeling of multilayer granitoid intrusions: Implications for the building and thermal evolution of the Central System batholith, Iberian Massif, Spain. *Lithos*, *175–176*, 104–123. https://doi.org/10.1016/J.LITHOS.2013.05.006

Díaz-Alvarado, J., Fernández, C., Díaz-Azpiroz, M., Castro, A., & Moreno-Ventas, I. (2012). Fabric evidence for granodiorite emplacement with extensional shear zones in the Variscan Gredos massif (Spanish Central System). *Journal of Structural Geology*, *42*, 74–90. https://doi.org/10.1016/j.jsg.2012.06.012

Diez Balda, M. A., García Casquero, J. L., & Alonso, P. (1990). Cizallamientos subverticales posteriores a la segunda fase de deformación hercínica al sur de Salamanca. *Revista de la Sociedad Geologica de Espana*, *3*, 117–125.

Diez Balda, M. A., Martinez Catalan, J. R., & Ayarza Arribas, P. (1995). Syn-collisional extensional collapse parallel to the orogenic trend in a domain of steep tectonics: The Salamanca Detachment Zone (Central Iberian Zone, Spain). *Journal of Structural Geology*, *17*(2), 163–182. https://doi.org/10.1016/0191-8141(94)E0042-W

Díez Fernández, R., & Pereira, M. F. (2016). Extensional orogenic collapse captured by strike-slip tectonics: Constraints from structural geology and U-Pb geochronology of the Pinhel shear zone (Variscan orogen, Iberian Massif). *Tectonophysics*, *691*, 290–310. https://doi.org/10.1016/j.tecto.2016.10.023

Díez Fernández, R. D., & Pereira, M. F. (2017). Strike-slip shear zones of the Iberian Massif: Are they coeval? *Lithosphere*, *9*(5), 726–744. https://doi.org/10.1130/L648.1

Diez-Montes, A., Martínez Catalán, J. R., & Bellido Mulas, F. (2010). Role of the Ollo de Sapo massive felsic volcanism of NW Iberia in the Early Ordovician dynamics of northern Gondwana. *Gondwana Research*, *17*(2–3), 363–376. https://doi.org/10.1016/j.gr.2009.09.001

Doblas, M. (1991). Late Hercynian extensional and transcurrent tectonics in Central Iberia. *Tectonophysics*, *191*, 325–334. https://doi.org/10.1016/0040-1951(91)90065-z

Doblas, M., López-Ruiz, J., Oyarzun, R., Mahecha, V., Moya, Y. S., Hoyos, M., et al. (1994). Extensional tectonics in the central Iberian Peninsula during the Variscan to Alpine transition. *Tectonophysics*, *238*(1–4), 95–116. https://doi.org/10.1016/0040-1951(94)90051-5

Doblas, M., Oyarzun, R., Sopeña, A., López Ruiz, J., Capote, R., Hernández Enrile, J. L., et al. (1994). Variscan-late Variscan-early Alpine progressive extensional collapse of central Spain. *Geodinamica Acta*, *7*(1), 1–14. https://doi.org/10.1080/09853111.1994.11105255

Dunn, A. M., Reynolds, P. H., Clarke, D. B., & Ugidos, J. M. (1998). A comparison of the age and composition of the Shelburne dyke, Nova Scotia, and the Messejana dyke, Spain. *Canadian Journal of Earth Sciences*, *35*(10), 1110–1115. https://doi.org/10.1139/e98-058

Ehsan, S. A., Carbonell, R., Ayarza, P., Martí, D., Martínez Poyatos, D., Simancas, J. F., et al. (2015). Lithospheric velocity model across the Southern Central Iberian Zone (Variscan Iberian Massif): The ALCUDIA wide-angle seismic reflection transect. *Tectonics*, *34*(3), 535–554. https://doi.org/10.1002/2014TC003661

Ehsan, S. A., Carbonell, R., Ayarza, P., Martí, D., Pérez-Estaún, A., Martínez-Poyatos, D. J., et al. (2014). Crustal deformation styles along the reprocessed deep seismic reflection transect of the Central Iberian Zone (Iberian Peninsula). *Tectonophysics*, *621*, 159–174. https://doi.org/10.1016/j.tecto.2014.02.014

Escuder Viruete, J., Arenas, R., & Martínez Catalán, J. R. (1994). Tectonothermal evolution associated with Variscan crustal extension in the Tormes Gneiss Dome (NW Salamanca, Iberian Massif, Spain). *Tectonophysics*, *238*(1–4), 117–138. https://doi.org/10.1016/0040-1951(94)90052-3

Escuder Viruete, J., Hernáiz Huerta, P. P., Valverde-Vaquero, P., Rodríguez Fernández, R., & Dunning, G. (1998). Variscan syncollisional extension in the Iberian Massif: Structural, metamorphic and geochronological evidence from the Somosierra sector of the Sierra de Guadarrama (Central Iberian Zone, Spain). *Tectonophysics*, *290*(1–2), 87–109. https://doi.org/10.1016/S0040-1951(98)00014-6

Escuder Viruete, J., Indares, A., & Arenas, A. R. (2000). P-T paths derived from garnet growth zoning in an extensional setting: An example from the Tormes Gneiss Dome (Iberian Massif, Spain). *Journal of Petrology*, *41*. https://doi.org/10.1093/petrology/41.10.1489

Fernández-Lozano, J., Sokoutis, D., Willingshofer, E., Cloetingh, S., & De Vicente, G. (2011). Cenozoic deformation of Iberia: A model for intraplate mountain building and basin development based on analogue modeling. *Tectonics*, *30*(1), 1–25. https://doi.org/10.1029/2010TC002719

Finlayson, D. M., Collins, C. D. N., & Lock, J. (1984). P-wave velocity features of the lithosphere under the Eromanga Basin, Eastern Australia, including a prominent MID-crustal (Conrad?) discontinuity. *Tectonophysics*, *101*, 267–291. https://doi.org/10.1016/0040-1951(84)90117-3

Flecha, I., Carbonell, R., Zeyen, H., Martí, D., Palomeras, I., Simancas, F., & Pérez-Estaún, A. (2006). Imaging granitic plutons along the IBER-SEIS profile. *Tectonophysics*, *420*(1–2), 37–47. https://doi.org/10.1016/j.tecto.2006.01.019

Franke, W., & Dulce, J. C. (2017). Back to sender: Tectonic accretion and recycling of Baltica-derived Devonian clastic sediments in the Rheno-Hercynian Variscides. *International Journal of Earth Sciences*, *106*(1), 377–386. https://doi.org/10.1007/s00531-016-1408-y

Gallastegui, J., Pulgar, J. A., & Gallart, J. (2016). Alpine tectonic wedging and crustal delamination in the Cantabrian Mountains (NW Spain). *Solid Earth*, *7*(4). https://doi.org/10.5194/se-7-1043-2016

García-Arias, M., Díez-Montes, A., Villaseca, C., & Blanco-Quintero, I. F. (2018). The Cambro-Ordovician Ollo de Sapo magmatism in the Iberian Massif and its Variscan evolution: A review. *Earth-Science Reviews*, *176*, 345–372. https://doi.org/10.1016/j.earscirev.2017.11.004

Giner-Robles, J. L., Pérez-López, R., Silva, P. G., Jiménez-Díaz, A., & Rodríguez-Pascua, M. A. (2012). Recent tectonic model for the Upper Tagus Basin (central Spain). *Journal of Iberian Geology*, *38*(1), 113–126. https://doi.org/10.5209/rev_jige.2012.v38.n1.39208

Gómez-Ortiz, D., Tejero-López, R., Babín-Vich, R., & Rivas-Ponce, A. (2005). Crustal density structure in the Spanish Central System derived from gravity data analysis (Central Spain). *Tectonophysics*, *403*(1–4), 131–149. https://doi.org/10.1016/j.tecto.2005.04.006

González-Clavijo, E., & Díez Montes, A. (2008). Procesos tardi-variscos en la Zona Centro Ibérica. Las bandas de cizalla subverticales del Domo del Tormes. *Geotemas*, *10*, 1567–5172.

Gutiérrez-Alonso, G., Collins, A. S., Fernández-Suárez, J., Pastor-Galán, D., González-Clavijo, E., Jourdan, F., et al. (2015). Dating of lithospheric buckling: [40]Ar/[39]Ar ages of syn-orocline strike–slip shear zones in northwestern Iberia. *Tectonophysics*, *643*, 44–54. https://doi.org/10.1016/j.tecto.2014.12.009

Gutiérrez-Elorza, M., Garcia-Ruiz, J. M., Goy, J. L., Gracia, F. J., Gutiérrez-Santolalla, F., Marti, C., et al. (2002). Quaternary. In W. Gibbons, & T. Moreno (Eds.), *The Geology of Spain*. London.

Gutiérrez-Marco, J. C., Piçarra, J. M., Meireles, C. A., Cózar, P., García-Bellido, D. C., Pereira, Z., et al. (2019). Early Ordovician–Devonian passive margin stage in the Gondwanan Units of the Iberian Massif. In J. T. O. C. Quesada (Ed.), *The geology of Iberia: A geodynamic approach*. *Regional Geology Reviews* (pp. 75–98). https://doi.org/10.1007/978-3-030-10519-8_3

Hernández Enrile, J. L. (1991). Extensional tectonics of the Toledo ductile-brittle shear zone, central Iberian Massif. *Tectonophysics*, *191*(3–4), 311–324. https://doi.org/10.1016/0040-1951(91)90064-Y

Heron, P. J., Pysklywec, R. N., & Stephenson, R. (2016). Identifying mantle lithosphere inheritance in controlling intraplate orogenesis. *Journal of Geophysical Research: Solid Earth*, *121*(9), 6966–6987. https://doi.org/10.1002/2016JB013460

Jammes, S., Huismans, R. S., & Muñoz, J. A. (2014). Lateral variation in structural style of mountain building: Controls of rheological and rift inheritance. *Terra Nova*, *26*(3), 201–207. https://doi.org/10.1111/ter.12087

Jarvis, A., Reuter, H. I., Nelson, A., & Guevara, E. (2008). International Centre for Tropical Agriculture (CIAT). In *Hole-filled seamless SRTM data V4*. Retrieved from https://srtm.csi.cgiar.org

Karampaglidis, T., Benito-Calvo, A., Rodés, A., Braucher, R., Pérez-González, A., Pares, J., et al. (2020). Pliocene endorheic-exhoreic drainage transition of the Cenozoic Madrid Basin (Central Spain). *Global and Planetary Change*, *194*, 103295. https://doi.org/10.1016/j.gloplacha.2020.103295

Kroner, U., Roscher, M., & Romer, R. L. (2016). Ancient plate kinematics derived from the deformation pattern of continental crust: Paleo- and Neo-Tethys opening coeval with prolonged Gondwana–Laurussia convergence. *Tectonophysics*, *681*, 220–233. https://doi.org/10.1016/j.tecto.2016.03.034

Labaume, P., Meresse, F., Jolivet, M., Teixell, A., & Lahfid, A. (2016). Tectonothermal history of an exhumed thrust-sheet-top basin: An example from the south Pyrenean thrust belt. *Tectonics*, *35*(5), 1280–1313. https://doi.org/10.1002/2016TC004192

López-Gómez, J., Alonso-Azcárate, J., Arche, A., Arribas, J., Fernández Barrenechea, J., Borruel-Abadía, V., et al. (2019). Permian-Triassic rifting stage. In C. Quesada, & J. Oliveira (Eds.), *The geology of Iberia: A geodynamic approach. Regional Geology Reviews*. Cham: Springer. https://doi.org/10.1007/978-3-030-11295-0_3

Macchiavelli, C., Vergés, J., Schettino, A., Fernàndez, M., Turco, E., Casciello, E., et al. (2017). A new Southern North Atlantic Isochron map: Insights into the drift of the Iberian plate since the Late Cretaceous. *Journal of Geophysical Research: Solid Earth*, *122*(12), 9603–9626. https://doi.org/10.1002/2017JB014769

Manghnani, M. H., Ramananantoandro, R., & Clark, S. P., Jr. (1974). Compressional and shear wave velocities in granulite facies rocks and eclogites to 10 kbar. *Journal of Geophysical Research (1896-1977)*, *79*(35), 5427–5446. https://doi.org/10.1029/JB079i035p05427

Martín-Chivelet, J., López-Gómez, J., Aguado, R., Arias, C., Arribas, J., Arribas, M. E., et al. (2019). The Late Jurassic–Early Cretaceous rifting. In C. Quesada, & J. Oliveira (Eds.), *The geology of Iberia: A geodynamic approach. Regional geology Reviews*. Cham: Springer. https://doi.org/10.1007/978-3-030-11295-0_5

Martínez Catalán, J. R. (2011). Are the oroclines of the Variscan belt related to late Variscan strike-slip tectonics? *Terra Nova*, *23*, 241–247. https://doi.org/10.1111/j.1365-3121.2011.01005.x

Martínez Catalán, J. R. (2012). The Central Iberian arc, an orocline centered in the Iberian Massif and some implications for the Variscan belt. *International Journal of Earth Sciences*, *101*(5). https://doi.org/10.1007/s00531-011-0715-6

Martínez Catalán, J. R., Arenas, R., Díaz García, F., Cuadra, P. G., Gómez-Barreiro, J., Abati, J., et al. (2007). Space and time in the tectonic evolution of the northwestern Iberian Massif: Implications for the Variscan belt. *Memoir of the Geological Society of America*, *200*(21), 403–423. https://doi.org/10.1130/2007.1200(21)

Martínez Catalán, J. R., Arenas, R., García, F. D., & Abati, J. (1997). Variscan accretionary complex of northwest Iberia: Terrane correlation succession of tectonothermal events. *Geology*, *25*(12), 1103–1106. https://doi.org/10.1130/0091-7613(1997)025<1103:VACONI>2.3.CO;2

Martínez Catalán, J. R., Hatcher, R. D., Jr., Arenas, R., & García, F. D. (2002). *Variscan-Appalachian dynamics: The building of the late Paleozoic basement*. Geological Society of America. https://doi.org/10.1130/SPE364

Martínez Catalán, J. R., Rubio Pascual, F. J., Díez Montes, A., Díez Fernández, R., Gómez Barreiro, J., Dias Da Silva, Í., et al. (2014). The late Variscan HT/LP metamorphic event in NW and Central Iberia: Relationships to crustal thickening, extension, orocline development and crustal evolution. *Geological Society Special Publication*, *405*(1), 225–247. https://doi.org/10.1144/SP405.1

Martínez Poyatos, D., Carbonell, R., Palomeras, I., Simancas, J. F., Ayarza, P., Martí, D., et al. (2012). Imaging the crustal structure of the Central Iberian Zone (Variscan Belt): The ALCUDIA deep seismic reflection transect. *Tectonics*, *31*(3), 1–21. https://doi.org/10.1029/2011TC002995

Martín-Serrano, A. (1991). La definición y el encajamiento de la red fluvial actual sobre el Macizo Herpérico en el marco de su geodinámica Alpina. *Revista de la Sociedad Geologica de Espana*, *4*, 337–351.

Masini, E., Manatschal, G., Tugend, J., Mohn, G., & Flament, J. M. (2014). The tectono-sedimentary evolution of a hyper-extended rift basin: The example of the Arzacq-Mauléon rift system (Western Pyrenees, SW France). *International Journal of Earth Sciences*, *103*(6), 1569–1596. https://doi.org/10.1007/s00531-014-1023-8

Matte, P. (1991). Accretionary history and crustal evolution of the Variscan belt in Western Europe. *Tectonophysics*, *196*(3–4), 309–337. https://doi.org/10.1016/0040-1951(91)90328-P

Matte, P. (2001). The Variscan collage and orogeny (480-290 Ma) and the tectonic definition of the Armorica microplate: A review. *Terra Nova*, *13*(2), 122–128. https://doi.org/10.1046/j.1365-3121.2001.00327.x

Miller, R. B., & Paterson, S. R. (2001). Influence of lithological heterogeneity, mechanical anisotropy, and magmatism on the rheology of an arc, North Cascades, Washington. *Tectonophysics*, *342*(3–4), 351–370. https://doi.org/10.1016/S0040-1951(01)00170-6

Montero, P., Bea, F., Zinger, T. F., Scarrow, J. H., Molina, J. F., & Whitehouse, M. (2004). 55 million years of continuous anatexis in Central Iberia: Single-zircon dating of the Peña Negra Complex. *Journal of the Geological Society*, *161*(2), 255–263. https://doi.org/10.1144/0016-764903-024

Montero, P., Talavera, C., Bea, F., Lodeiro, F. G., & Whitehouse, M. J. (2009). Zircon geochronology of the Ollo de Sapo Formation and the age of the Cambro-Ordovician rifting in Iberia. *The Journal of Geology*, *117*(2), 174–191. https://doi.org/10.1086/595017

Mouthereau, F., Watts, A. B., & Burov, E. (2013). Structure of orogenic belts controlled by lithosphere age. *Nature Geoscience*, *6*(9), 785–789. https://doi.org/10.1038/ngeo1902

Muñoz, J. A. (1992). Evolution of a continental collision belt: ECORS-Pyrenees crustal balanced cross-section. In: In K. R. McClay, (ed.) *Thrust tectonics* (pp. 235–246). London: Chapman and Hall.

Muñoz-Martín, A., De Vicente, G., Fernández-Lozano, J., Cloetingh, S., Willingshofer, E., Sokoutis, D., & Beekman, F. (2010). Spectral analysis of the gravity and elevation along the Western Africa-Eurasia plate tectonic limit: Continental versus oceanic lithospheric folding signals. *Tectonophysics*, *495*(3–4), 298–314. https://doi.org/10.1016/j.tecto.2010.09.036

Nance, R. D., Gutiérrez-Alonso, G., Keppie, J. D., Linnemann, U., Murphy, J. B., Quesada, C., et al. (2012). A brief history of the Rheic Ocean. *Geoscience Frontiers*, *3*(2), 125–135. https://doi.org/10.1016/j.gsf.2011.11.008

O'Neill, H. S. C. (1981). The transition between spinel lherzolite and garnet lherzolite, and its use as a Geobarometer. *Contributions to Mineralogy and Petrology*, *77*(2), 185–194. https://doi.org/10.1007/BF00636522

Orejana, D., Villaseca, C., Billström, K., & Paterson, B. A. (2008). Petrogenesis of Permian alkaline lamprophyres and diabases from the Spanish Central System and their geodynamic context within Western Europe. *Contributions to Mineralogy and Petrology*, *156*(4). https://doi.org/10.1007/s00410-008-0297-x

Orejana, D., Villaseca, C., Pérez-Soba, C., López-García, J. A., & Billström, K. (2009). The Variscan gabbros from the Spanish Central System: A case for crustal recycling in the sub-continental lithospheric mantle? *Lithos*, *110*(1–4), 262–276. https://doi.org/10.1016/J.LITHOS.2009.01.003

Orejana, D., Villaseca, C., Valverde-Vaquero, P., Belousova, E. A., & Armstrong, R. A. (2012). U-Pb geochronology and zircon composition of late Variscan S- and I-type granitoids from the Spanish Central System batholith. *International Journal of Earth Sciences*, *101*(7), 1789–1815. https://doi.org/10.1007/s00531-012-0750-y

Palomeras, I., Ayarza, P., Andrés, J., Álvarez-Valero, A. M., Gómez-Barreiro, J., Díaz, J., et al. (2021). Mapping and interpreting the uppermost mantle reflectivity beneath Central and South-West Iberia. *Journal of Geophysical Research: Solid Earth*.

Palomeras, I., Carbonell, R., Flecha, I., Simancas, F., Ayarza, P., Matas, J., et al. (2009). Nature of the lithosphere across the Variscan orogen of SW Iberia: Dense wide-angle seismic reflection data. *Journal of Geophysical Research: Solid Earth*, *114*(2), 1–29. https://doi.org/10.1029/2007JB005050

Palomeras, I., Ehsan, S. A., Martínez Poyatos, D. J., Ayarza, P., Martí, D., Carbonell, R., et al. (2021). Seismic structure and composition of the southern central Iberian crust: The ALCUDIA wide angle seismic reflection transect. *Tectonophysics*, *820*. https://doi.org/10.1016/j.tecto.2021.229114

Pereira Gómez, M. D., & Rodríguez Alonso, M. D. (2000). Duality of cordierite granites related to melt-restite segregation in the peña negra anatectic complex, Central Spain. *The Canadian Mineralogist*, *38*(6), 1329–1346.

Pérez-Cáceres, I., Martínez Poyatos, D., Simancas, J. F., & Azor, A. (2017). Testing the Avalonian affinity of the South Portuguese Zone and the Neoproterozoic evolution of SW Iberia through detrital zircon populations. *Gondwana Research*, 177–192. https://doi.org/10.1016/j.gr.2016.10.010

Pérez-Estaún, A., Bastida, F., Alonso, J. L., Marquínez, J., Aller, J., Alvarez-Marrón, J., et al. (1988). A thin-skinned tectonics model for an arcuate fold and thrust belt: The Cantabrian Zone (Variscan Ibero-Armorican Arc). *Tectonics*, *7*(3), 517–537. https://doi.org/10.1029/TC007i003p00517

Pérez-Estaún, A., & Bea, F. (2004). Macizo Ibérico. In J. A. Vera (Ed.), *Geología de España* (pp. 19–230). SGE-IGME.

Pérez-González, A. (1994). Depresión del Tajo. In M. Gutiérrez Elorza (Ed.), *Geomorfología de España (Editorial)* (pp. 189–388). Madrid.

Pous, J., Muñoz-Martín, A., Olaiz Campos, A. J., Seillé, H., & DeVicente, G. (2012). Análisis de la estructura alpina de la corteza del centro de la Península Ibérica: Una sección Magneto-Telúrica a través del Sistema Central (Sierra de Gredos). *Geotemas*, *13*, 4–8.

Pulgar, J. A., Gallart, J., Fernandez-Viejo, G., Perez-Estaun, A., Alvarez-Marron, J., & Group, E. (1996). Seismic image of the Cantabrian Mountains in the Western extension of the Pyrenees from integrated ESCIN reflection and refraction data. *Tectonophysics*, *264*(1–4), 1–19. https://doi.org/10.1016/S0040-1951(96)00114-X

Quijada, I. E., Suarez-Gonzalez, P., Benito, M. I., & Mas, R. (2014). New insights on stratigraphy and sedimentology of the Oncala Group (eastern Cameros Basin): Implications for the paleogeographic reconstruction of Iberia at Berriasian times. *Journal of Iberian Geology*, *39*(2). https://doi.org/10.5209/rev_jige.2013.v39.n2.42503

Quintana, L., Pulgar, J. A., & Alonso, J. L. (2015). Displacement transfer from borders to interior of a plate: A crustal transect of Iberia. *Tectonophysics*, *663*, 378–398. https://doi.org/10.1016/j.tecto.2015.08.046

Rodríguez Alonso, M. D., Díez Balda, M. A., Perejón, A., Pieren, A., Liñán, E., López Díaz, F., et al. (2004). *La secuencia litoestratigráfica del Neoproterozoico-Cámbrico Inferior*. Geología de España.

Rodríguez Fernández, L. R., López Olmedo, F., Oliveira, J. T., Matas, J., Martín-Serrano, A., Martín Parra, L. M., et al. (2015). Mapa Geológico de España y Portugal E 1: 1.000.000. In L. R. Rodríguez Fernández & J. T. Oliveira (Eds.), *IGME-LNEG*.

Rodríguez-Pascua, M. A., Silva, P. G., Perucha, M. A., Giner-Robles, J. L., Heras, C., Bastida, A. B., et al. (2016). Seismically induced lique-faction structures in La Magdalena archaeological site, the 4th century AD Roman Complutum (Madrid, Spain). *Sedimentary Geology*, *344*, 34–46. https://doi.org/10.1016/j.sedgeo.2016.01.025

Rodríguez-Rodríguez, L., Antón, L., Rodés, Á., Pallàs, R., García-Castellanos, D., Jiménez-Munt, I., et al. (2020). Dates and rates of endo-exorheic drainage development: Insights from fluvial terraces (Duero River, Iberian Peninsula). *Global and Planetary Change*, *193*, 103271. https://doi.org/10.1016/j.gloplacha.2020.103271

Rosenbaum, G., Lister, G. S., & Duboz, C. (2002). Relative motions of Africa, Iberia and Europe during Alpine orogeny. *Tectonophysics*, *359*(1–2), 117–129. https://doi.org/10.1016/S0040-1951(02)00442-0

Rubio Pascual, F. J., Arenas, R., Martínez Catalán, J. R., Rodríguez Fernández, L. R., & Wijbrans, J. R. (2013). Thickening and exhumation of the Variscan roots in the Iberian Central System: Tectonothermal processes and 40Ar/39Ar ages. *Tectonophysics*, *587*, 207–221. https://doi.org/10.1016/j.tecto.2012.10.005

Rubio Pascual, F. J., López-Carmona, A., & Arenas, R. (2016). Thickening vs. extension in the Variscan belt: P–T modelling in the Central Iberian autochthon. *Tectonophysics*, *681*, 144–158. https://doi.org/10.1016/j.tecto.2016.02.033

Sell, I., Poupeau, G., Casquet, C., Galindo, C., & González-Casado, J. M. (1995). Exhumación alpina del bloque morfotectónico Pedriza-La Cabrera (Sierra de Guadarrama, Sistema Central Español): Potencialidad de la termocronometría por trazas de fisión en apatitos. *Geogaceta*, *18*, 23–26.

Silva, P. G., Roquero, E., López-Recio, M., Huerta, P., & Martínez-Graña, A. M. (2017). Chronology of fluvial terrace sequences for large Atlantic rivers in the Iberian Peninsula (Upper Tagus and Duero drainage basins, Central Spain). *Quaternary Science Reviews*, *166*, 188–203. https://doi.org/10.1016/j.quascirev.2016.05.027

Simancas, J. F. (2019). Variscan cycle. In *The geology of Iberia: A geodynamic approach* (pp. 1–25). Cham: Springer. https://doi.org/10.1007/978-3-030-10519-8_1

Simancas, J. F., Ayarza, P., Azor, A., Carbonell, R., Martínez Poyatos, D., Pérez-Estaún, A., & González Lodeiro, F. (2013). A seismic geotraverse across the Iberian Variscides: Orogenic shortening, collisional magmatism, and orocline development. *Tectonics*, *32*(3), 417–432. https://doi.org/10.1002/tect.20035

Sokoutis, D., & Willingshofer, E. (2011). Decoupling during continental collision and intra-plate deformation. *Earth and Planetary Science Letters*, *305*(3–4), 435–444. https://doi.org/10.1016/j.epsl.2011.03.028

Stephenson, R., Egholm, D. L., Nielsen, S. B., & Stovba, S. M. (2009). Role of thermal refraction in localizing intraplate deformation in southeastern Ukraine. *Nature Geoscience*, *2*(4), 290–293. https://doi.org/10.1038/ngeo479

Suriñach, E., & Vegas, R. (1988). Lateral inhomogeneities of the Hercynian crust in central Spain. *Physics of the Earth and Planetary Interiors*, *51*(1–3), 226–234. https://doi.org/10.1016/0031-9201(88)90049-0

Talavera, C., Martínez Poyatos, D., & González Lodeiro, F. (2015). SHRIMP U–Pb geochronological constraints on the timing of the intra-Alcudian (Cadomian) angular unconformity in the Central Iberian Zone (Iberian Massif, Spain). *International Journal of Earth Sciences*, *104*(7), 1739–1757. https://doi.org/10.1007/s00531-015-1171-5

Talavera, C., Montero, P., Martínez Poyatos, D., & Williams, I. S. (2012). Ediacaran to Lower Ordovician age for rocks ascribed to the Schist-Graywacke Complex (Iberian Massif, Spain): Evidence from detrital zircon SHRIMP U-Pb geochronology. *Gondwana Research*, *22*(3–4), 928–942. https://doi.org/10.1016/j.gr.2012.03.008

Teixell, A., & García-Sansegundo, J. (1995). Estructura del sector central de la Cuenca de Jaca (Pirineos meridionales). *Revista de la Sociedad Geologica de Espana*, *8*(3), 215–228.

Teixell, A., Labaume, P., Ayarza, P., Espurt, N., de Saint Blanquat, M., & Lagabrielle, Y. (2018). Crustal structure and evolution of the Pyrenean-Cantabrian belt: A review and new interpretations from recent concepts and data. *Tectonophysics*, *724–725*, 146–170. https://doi.org/10.1016/j.tecto.2018.01.009

Teixell, A., Labaume, P., & Lagabrielle, Y. (2016). The crustal evolution of the west-central Pyrenees revisited: Inferences from a new kinematic scenario. *Comptes Rendus Geoscience*, *348*(3–4), 257–267. https://doi.org/10.1016/j.crte.2015.10.010

Torne, M., Fernàndez, M., Vergés, J., Ayala, C., Salas, M. C., Jimenez-Munt, I., et al. (2015). Crust and mantle lithospheric structure of the Iberian Peninsula deduced from potential field modeling and thermal analysis. *Tectonophysics*, *663*, 419–433. https://doi.org/10.1016/j.tecto.2015.06.003

Vegas, R. (2000). The intrusion of the Plasencia (Messejana) dike as part of the Circum-Atlantic Early Jurassic magmatism: Tectonic implications in the southwestern Iberian peninsula. *Geogaceta*, *27*, 175–178.

Vegas, R., & Suriñach, E. (1987). Engrosamiento de la corteza y relieve intraplaca en el centro de Iberian. *Geogaceta*, *2*, 40–42.

Vegas, R., Vázquez, J. T., Suriñach, E., & Marcos, A. (1990). Model of distributed deformation, block rotations and crustal thickening for the formation of the Spanish Central System. *Tectonophysics*, *184*(3–4), 367–378. https://doi.org/10.1016/0040-1951(90)90449-I

Villamor, M. P. (2002). *Cinemática terciaria y cuaternaria de la falla de Alentejo-Plasencia y su influencia en la peligrosidad sísmica del interior de la Península Ibérica*. Universidad Complutense de Madrid.

Villamor, M. P., Stirling, M. W., Tsige Aga, M., Berryman, K. R., Martínez Díaz, J. J., & Martín-González, F. (2012). Contribution of active faults in the intraplate area of Iberia to seismic hazard: The Alentejo-Plasencia Fault. *Journal of Iberian Geology*, *38*(1), 85–111.

Villamor, P., Capote, R., & Tsige, M. (1996). Actividad neotectónica de la falla de Alentejo-Plasencia en Extremadura (Macizo Hespérico). *Geogaceta*, *20*(4), 925–928.

Villaseca, C., Downes, H., Pin, C., & Barbero, L. (1999). Nature and composition of the lower continental crust in Central Spain and the granulite-granite linkage: Inferences from granulitic xenoliths. *Journal of Petrology*, *40*(10), 1465–1496. https://doi.org/10.1093/petroj/40.10.1465

Villaseca, C., & Herreros, V. (2000). A sustained felsic magmatic system: The Hercynian granitic batholith of the Spanish Central System. *Special Paper of the Geological Society of America*, *350*(91), 207–219. https://doi.org/10.1130/0-8137-2350-7.207

Villaseca, C., Orejana, D., & Belousova, E. A. (2012). Recycled metaigneous crustal sources for S- and I-type Variscan granitoids from the Spanish Central System batholith: Constraints from Hf isotope zircon composition. *Lithos*, *153*, 84–93. https://doi.org/10.1016/j.lithos.2012.03.024

Weil, A., Pastor-Galán, D., Johnston, S. T., & Gutiérrez-Alonso, G. (2019). Late/Post Variscan orocline formation and widespread magmatism. In *The geology of Iberia: A geodynamic approach* (pp. 307–348). Cham: Springer. https://doi.org/10.1007/978-3-030-10519-8_14

Wever, T. (1989). The Conrad discontinuity and the top of the reflective lower crust-do they coincide? *Tectonophysics*, *157*(1–3), 39–58. https://doi.org/10.1016/0040-1951(89)90339-9

Wilson, M. (1997). Thermal evolution of the Central Atlantic passive margins: Continental break-up above a Mesozoic super-plume. *Journal of the Geological Society*, *154*, 491–495. https://doi.org/10.1144/gsjgs.154.3.0491

Wilson, R. W., Houseman, G. A., Buiter, S. J. H., McCaffrey, K. J. W., & Doré, A. G. (2019). Fifty years of the Wilson cycle concept in plate tectonics: An overview. *Geological Society Special Publication*, *470*(1), 1–17. https://doi.org/10.1144/SP470-2019-58

Zeck, H. P., Wingate, M. T. D., & Pooley, G. (2007). Ion microprobe U-Pb zircon geochronology of a late tectonic granitic-gabbroic rock complex within the Hercynian Iberian belt. *Geological Magazine*, *144*(1), 157–177. https://doi.org/10.1017/S0016756806002652

Zelt, C., & Smith, R. (1992). Seismic traveltime inversion for 2-D crustal velocity structure. *Geophysical Journal International*, *108*(1), 16–34. https://doi.org/10.1111/j.1365-246X.1992.tb00836.x

Ziegler, P. A., Van Wees, J. D., & Cloetingh, S. (1998). Mechanical controls on collision-related compressional intraplate deformation. *Tectonophysics*, *300*(1–4), 103–129. https://doi.org/10.1016/S0040-1951(98)00236-4